Department of Physics and Astronomy

Msc Thesis

Small animal irradiation using the MARS Spectral CT

Daniel Kim

(Kwang Hyuk Kim)

Supervision: Professor Phil Butler (Physics, UC)

Dr. Anthony Butler (Otago), Dr. Juan Canales (Psychology, UC)

February 2013

Abstract

This thesis reports on a novel use of the Medipix All Resolution System (MARS) Spectral CT scanner as a platform of small animal irradiation. Irradiation from the x-ray source in the scanner was used to inhibit the growth and recovery of neurons in rats. The goal is to extrapolate the relationship between stem cells and memory and functional behaviours. Specific developments were carried out prior to the irradiation of live rats. A live rat holder was designed and built to provide a setup stable enough for fixing the position of the rats head. This was achieved by integrating a three piece bar system into the holder to hold the head from both ears and nose. To quantify the absorbed dose, x-ray exposures were measured using a calibrated ion chamber and were used to generate a depth dose curve with sheets of Perspex layers and radiochromic films. This curve is presumed to simulate the dose inside the rat‘s head.

To target a sub region of interest within the rat‘s brain, specific anatomical landmarks were investigated for the design of the lead collimators. The position of the sub volume, the hippocampus, was located through a combination of anatomical landmarks and x-ray transmission images of the rat‘s head. Bregma and the interaural line were used to numerically plot out the co-ordinates of the dorsal and ventral hippocampus which was then translated onto the lead collimators.

The x-ray transmission images of euthanized rats were used as a guide to locate the dorsal and ventral hippocampuses. Bregma and the interaural line were the main anatomical landmarks which were used for the design of the lead collimators to be placed around the head. Three pilot rats were irradiated with the designed holder and collimators. The point dose to the hippocampus was calculated using the simulated depth dose curve. Post irradiation status of the neurogenesis was assessed three weeks after the treatment. However only one of the three rats showed a significant reduction in the number of neurons in the hippocampus emphasizing the room for more improvement in the physical setup of the irradiation.

Acknowledgement

As a part of my thesis, I would like to mention and thank some of the people that have helped me throughout this year. First of all I would like to thank Professor Phil Butler and Dr. Anthony Butler for giving me the opportunity to carry out this project and become part of the MARS group. Also extra thanks to Professor Phil Butler for being my senior supervisor and also through his ongoing support and input in this thesis.

I would also like to thank all the people in the MARS team. I have found many new friends and it was a real pleasure to be part of many discussions and work that have been going on throughout the year. Special thanks to Dr. Stephen Bell who was always at the lab for assistance and making the scanners more user friendly. His input into the group has been tremendous and I wish him all the best.

Dr. Juan Canales and Sahina (PHD candidate, Psychology) deserve special thanks for collaborate work on this unique project and educating me to understand a little bit more about the brain and how it functions. Also Tom Judd (summer student) for giving me a big hand in the experiments that was performed. This work would never have been the same without them. Would also like to thank Graeme (Physics and Astronomy), Derek (Psychology) for their part in designing and building of the live rat holder for the experiment and providing essential equipments when needed.

It has been a humbling experience to be working with such enthusiastic people of various backgrounds and I wish everyone the very best in their professional and personal goals.

Contents

1 Introduction **1**

1.1 Purpose of the Project 1

1.2 The MARS Group 2

1.3 Small Animal Irradiation Research 3

1.4 Thesis Outline 3

2 Literature Review **5**

2.1 History and the Development of Computed Tomography 5

2.2 Small Animal Irradiation 6

2.3 Rat Brain Anatomy 7

2.4 Neurogenesis 8

2.5 Radiation Biology 9

2.6 Study of Radiation Induced Impairment of Hippocampal Neurogenesis 11

2.7 Small Animal Irradiation Setups 12

3 Methods and Materials **15**

3.1 MARS Spectral CT 15

3.2 Live Rat Holder 16

3.3 Ionization Chamber 17

3.4 Films 18

3.5 Perspex Phantom 20

3.6 Preparation of the Rats 22

3.7 Irradiation 22

4 Radiation Dosimetry **25**

4.1 Dosimtery 25

4.2 X-ray Production 26

4.3 Measurement using Ionization Chamber 27

4.4 Film Calibration 27

4.5 Depth Dose 31

5 X-ray Imaging of Rats **33**

5.1 X-ray Imaging 33

5.1.1 Rayleigh Scattering 34

5.1.2 Photoelectric Absorption 35

5.1.3 Compton Scattering 36

5.2 Anatomical Landmarks in the Rat Brain 37

5.3 MARS - CT Preview Mode 40

6 Rat Irradiation and Histology **47**

6.1 Irradiation 47

6.2 Histology 50

7 Conclusion **55**

7.1 Summary 55

7.2 Discussion 56

7.3 Future Outlook 57

7.4 Conclusion 57

References **59**

References 59

A User Interfaces **63**

List of Figures

2.1 *Figure showing the rat brain and the hippocampus. The labelled areas show the dorsal and ventral hippocampus which will be targeted during the irradiation of the rat.*(Khoshnazar et al., 2012) 7

2.2 *Showing the anatomy of a 290g Male Wistar Rat. The landmarks on the skull are clearly labelled along with the distances. It has been shown that there are minimal differences in the position of the landmarks between the rats of the same weight.*(Paxinos et al., 1985) 8

2.3 *Showing the proces of neurogenesis in adult rodent brain. It is a three step process; proliferation, migration and differentiation in the dentate gyrus of the hippocampus.* (Gage et al., 2008) 10

2.4 *Direct and indirect mechanism of the ionizing radiation interacting with the DNA. The ejected electrons by radiation can interact directly with base pairs of the DNA while indirect pathway utilizes the water molecules surrounding the DNA.* 11

2.5 *Small Animal Irradiation Research Platform (SARRP) developed at Johns Hopkins University.*(Matinfar et al., 2009) 13

2.6 *The micro-CT scanner modified by Stanford University to be used for small animal irradiation related studies. (a) shows the mechanical hexagonal collimator (b) the micro CT modified for small animal studies*(Rodriguez et al., 2009) 14

3.1 *MARS spectral CT located on the 4th floor Department of Physics and Astronomy. The shown scanner is the MARS-unit6, a version 4 scanner integrated with the 120kVp x-ray tube.* 16

3.2 *Showing the apparatus for specifically desgined to place a live rat inside the MARS CT machine for irradiation. It consists of two ear bars and an adjustable nose bar and also the lead collimators.* 17

3.3 *The mechanism of the ionization chamber. The sensitive area corresponds to the chamber filled with gas for ionization. The current from the electrodes are proprotional to the ionizing radiation dose* 18

3.4 *Raysafe® Xi. The ionization chamber is connected to the readout via usb. The chamber is of compact size for durability a* 19

3.5 *Showing a sheet of the Gafchromic® XR-QA. The chemical composition of the film and thickness is shown by the figure on the right* 20

3.6 *Showing the phantom of multiple layer of persex sheets. The phantom can easily be adjusted to insert Gafchromic® films between each layer to obtain a depth dose curve* 21

3.7 *Diagram showing the basic setup for the rat irradiation inside the scanner. Parallel opposing beam geometry is used where the x-ray is rotated 180 degrees to irradiate the opposite lateral side.* 23

4.1 *Basic diagram of the x-ray tube and the concept of how the x-rays are produced and emitted. (A) corresponds to the target anode while (C) is the heated filament for releasing electrons.* 26

4.2 *Graph showing the dose measured using Raysafe®-Xi at various current settings on MARS CT-6 at 120kVp* 28

4.3 *Figure showing pieces ofGafchromic® XR-QA exposed to x-ray at a range of different current settings from 0uA to 350uA* 29

4.4 *Figure showing a single piece of Gafchromic® XR-QA for analysis. The yellow box is used to specify a region of area in the exposed section to measure the mean greylevel using ImageJ* 29

4.5 *Graph showing the Gafchromic ® XR-QA characteristics curve. The curve is split into two regions; linear and shoulder. Measurements with Gafchromic films should always be performed within the linear region.* 31

4.6 *Graph showing the depth dose curve. This was obtained by fitting an exponential fit to the data obtained by measuring the radiation at different depths of Perspex usingGafchromic® XR-QA.* 32

5.1 *Diagram illustrating the photon interaction of Rayleigh scattering. The scattered photon has the same energy as the incident photon. (Bushberg et al., 2006)* 35

5.2 *Photoelectric absorption showing a 100keV photon interacting with an iodine atom. (Bushberg et al., 2006)* 36

5.3 *Compton scattering diagram. The incident photon energy is used to release the compton electron and the remaining photon energy is scattered at angle of ϕ. (Bushberg et al., 2006)* 37

5.4 *Plots showing the areas of the dorsal (a) and ventral (b) hippocampus relative to the position of the bregma and the interaural line.* 39

5.5 *Radiographic images of euthanized rat taken at Christchurch Women's Hospital. The stainless steel pins are attached to the bregma and lambda points on the skull. The yellow lines represent the area of the hippocampus.* 40

5.6 *Figure showing the geometrics of the x-ray tube. The image edges are suubject to magnifcation blurring, f, which is produced by the extended focal spot of the x-ray tube labelled as F. (Bushberg et al., 2006)* 42

5.7 *Figure showing the Medipix 3.1 Silicon Quad detector (Q12). The yellow dotted lines represent the narrow slice region on the detector which the x-ray transmission data is used to stitch and produce an extended x-ray transmission image.* 43

5.8 *Figures showing: (a) the original image produced from the MARS Preview Mode and (b) image showing the improved quality after applying the smoothing filter* 44

5.9 *Figure x-ray projection image taken from MARS CT-5 with the Medipix 3.1 silicon quad. The image shows an euthanized rat with steel pin attached to the bregma of the rats skull. Aluminium plate with grid pattern holes was placed around the rats head for geometric information.* 45

6.1 *The lead collimator used to confine the cone beam x-ray. The position of the x-ray hole was hand carved.* 48

6.2 *Close up photo of the rats head fixed with the ear bars and nose bars and also the collimators which are connected with the ear bars.* 49
6.3 *Figure showing the measurement of the depth of the hippocampus. The depth of the hippocampus on each hemispheres was measured from the same side.* . . 50
6.4 *Graph showing the depth dose curve with the labeled depths of the hippocampus at both hemispheres* 51
6.5 *Diagram illustrating the point dose rate from a single lateral beam in both hemispheres. The values will be flipped around with the x-ray source on the opposite side.* 51
6.6 *Showing the rat positioned inside the scanner fixed in place on the live animal holder. It is assumed that the position of the head held by the stereotaxic bars is in the centre of the opposing parallel beam geometry.* 52
6.7 *Light microscopy image of the brain section of the brain stained with DoublecortinX. (a) unirradiated control rat (b) irradiated rat showing small reduction in the number of neurons (c) a section in the irradiated rat brain which showed very low number of neurons showing signs of reduced neurogenesis.* . . 53

7.1 *The MARS-CR10 currently in its final stages of development. The gantry, (a) and (b), and the motorized shutters, (c), are shown.* 58

A.1 *Figure showing the graphical user interface used in the MARS Spectral CT. The current system has two scan modes; Preview Mode and Scan Mode.* . . . 63
A.2 *The main control panel used for setting up scans in the MARS Spectral CT. The Preview Mode requires the user to define the diameter, start position and length of the sample. The Run button is clicked to initate the scan.* 64

List of Tables

3.1 *Table showing the estimated values of the x-ray dose at different depths of Perspex measured using the Gafchromic® XR-QA* 21

4.1 *Table showing the dose measure using the Raysafe®-Xi ionization chamber at different x-ray current settings.* 27

4.2 *Table showing the dose measure using the Raysafe®-Xi ionization chamber at different x-ray current settings. The table also includes the mean grey value measured on the exposed Gafchromic ® XR-QA film.* 30

4.3 *Table showing the calculated values of the x-ray dose using the optical density of the exposed Gafchromic® XR-QA and its calibration curve.* 32

5.1 *Smoothing kernel that is convoluted with the image to produce a better quality image. This kernel is used to replace the central pixel values with the average pixel value of the surrounding pixels.* 43

CHAPTER 1

Introduction

This Master's thesis is based on the topic: small animal irradiation using the MARS Spectral CT. Since the discovery of clinical applications of x-ray, the uses of radiation have been mostly limited to medical imaging (radiology) and as a therapeutic approach for the treatment of tumours (oncology). However, due to the advances in technology it is now possible to use radiation as an approach for research in areas other than radiology and oncology. In particular selective targeting of certain anatomical sub volumes in the brain of animal models is of interest in order to switch off certain functionality which in turn enables researchers to investigate the effects.

This chapter introduces the purpose of the project and the Medipix All Resolution System (MARS) research team at the University of Canterbury. The applications of small animal irradiation and the potential field of research in which it may be used for human relevant clinical study is also covered. The last section outlines the content and the structure of the thesis.

1.1 Purpose of the Project

Small animal related experiments have become an important field for human related clinical studies. In particular, the experimental use of irradiation has become an emerging tool utilized by small animal researchers today. The MARS Spectral CT is a micro-CT originally

designed as a spectral imaging system for small animals and pathological specimens. However, the micro focus x-ray tube, silicon detector readout system and the rotating gantry of the micro-CT has the potential to be expanded towards the field of image guided radiotherapy. With the interest from the Department of Psychology, University of Canterbury, of using irradiation as a tool for the study of neurogenesis in rodent brains, the project was collaboratively performed to analyze the potential of the MARS scanner for this purpose. The collaborative project involved a multiple disciplinary of fields from physics, engineering to the issues of biology and psychology.

From the interests shown from various associates regarding therapy related applications, a new version, V5 of the CT scanner, MARS-CR1 Unit-10, is being developed by the MARS physics team. Unit-10 is integrated with an x-y translational stage and motorized shutters which are additional features that are designed to simplify therapy related experiments. The main purpose of this project will be used as an initial step of integrating the research team with therapy related applications and also with the upcoming MARS-CR1.

1.2 The MARS Group

The MARS research group is a multidisciplinary research group focusing on the development of a commercial small animal and pre clinical CT. This MARS CT is integrated with the Medipix detectors developed by a collaboration based at CERN, Geneva. The University of Canterbury is a member of the Medipix3 Collaboration (Butler & Butler, 2013). The novel features of the Medipix detector includes the ability to process the charge deposited by each of the x-ray photon and then measuring its energy for spectral imaging. The name, MARS Spectral CT, defines the unique combination of spectral imaging with computed tomography. The MARS research group is currently based at the University of Canterbury along with the University of Otago and their associated partners. Research includes a range of mathematical, clinical and experimental based approaches for the applications in diagnosing human related diseases and also detector related studies.

1.3 Small Animal Irradiation Research

Research based on small animal models can provide an increased understanding of human related health risks. Modelling of pathologies, disease progression and response to therapy are one of many various aspects that have been investigated through the versatility of small animal models. In particular, irradiation experiments using small animal models have recently been emphasized as the development of therapeutic and imaging technologies have allowed the field to propagate into unexplored areas of practice. A growing number of groups have dedicated their efforts into developing versatile small animal radiation research platforms and enabling research opportunities not only in the field of radiotherapy but also radiobiology, immunology and neuronal stem cell studies. The examples of the platforms that have been developed by the groups are covered in Chapter 3.

1.4 Thesis Outline

The thesis covers the research and the experimental process performed for the small animal irradiation using the MARS Spectral CT. The project was performed in collaboration with the Department of Psychology, University of Canterbury, for the study of neurogenesis and its relation with memory and function.

Chapter 2 is a review of the literature based on small animal irradiation. Basic principles such as radiation biology, structural anatomy of rats and process of neurogenesis will be covered along with the importance of the hippocampal irradiation related studies. The chapter will also include brief overview of the small animal radiotherapy setups developed by clinical research groups and some of the technical specifications that they have used in order to deliver radiation dose with high accuracy and precision.

Chapter 3 describes the equipment that was used during the experiments. Photographic images of the equipments are provided along with the relevant theory of how each one operates. The preparation of the rats and the experimental procedure of the irradiation of the rats is given at the end of this chapter.

Chapter 4 covers the basic theory of x-ray production and the dosimetry results obtained

from the MARS Spectral CT. The physical process of x-ray production through clinical x-ray tube is described and illustrated. Results obtained from dosimeters such as ionization chamber and Gafchromic® films are provided along with the performed analysis of the results. The dosimetric measurements were performed with the help from a local medical physicist, Dr Nick Cook, Canterbury District Health Board (CDHB).

In chapter 5, the theory of x-ray radiation is used to produce images will be explained. Clinical x-ray transmission images of euthanized rats are shown and compared with the transmission images taken through the MARS CT and the new preview mode scan. Anaotmical landmarks will also be explained and how it will be used to locate the hippocampus of the brain which cannot be seen through the transmission images.

Chapter 6 shows the results of the pilot study performed on three rats. This experimental trial was used to check the accuracy of the setup and whether the neurogenesis was inhibited. Although the trial produced mixed results, a positive result seen in one of rats showing significant reduction in the number of neuron cells is analyzed through light microscopy. The next will be to use my results in a more extensive psychology trial.

Chapter 7 discusses the overall objective of the thesis and evaluates the results obtained through the work. The chapter also provides recommendation of future tasks and improvements that could be made to achieve better experimental outcome. The conclusion of the thesis will also be a part of this chapter.

CHAPTER 2

Literature Review

This chapter reviews the platform of small animal irradiation and the pioneering studies that have been published in literatures. After a brief historical review of CT and the importance of small animal experiments, the chapter will be followed on by a summary of the basic biology involved with the project; anatomy of the rodent's head, process of neurogenesis and radiation biology. And finally the last section shows the examples of small animal irradiation platforms used and developed by clinical research groups. The hardware and technical details of the platforms are shown and summarised.

2.1 History and the Development of Computed Tomography

Since the early discovery of x-ray radiation by Wilhelm Roentgen in 1875, scientific innovations have been carried out throughout the usage of x-rays in medical practices and have lead to the invention of computed tomography (CT). In 1972, Godfrey Hounsfield and A.M. Cormack initiated a new era in diagnostic imaging through their work in developing the first computed tomography technique (Hounsfield, 1973). The cross sectional imaging technique has proven to be one of the greatest inventions in the field of medical engineering and radiology which eventually lead to the Nobel Prize being awarded to both Hounsfield and Cormack in 1979.

CT has undergone many generations of improvement due to the advances in our understanding of x-ray radiation, hardware and also mathematical algorithms used for image reconstruction. Hardware components such as x-ray tubes, detector technology and computer processors are some of the main aspects that have been influential in the evolution of this specific imaging modality. Modern generations of CT scanners include micro CT, phase contrast CT and spectral CT where material decomposition and coloured imaging have now become possible.

2.2 Small Animal Irradiation

Small animal radiotherapy platform is a young emerging field. The research has been of interest by many groups, albeit not all of them in the field of radiotherapy, indicating the immense research potential the field can provide. However due to the sophisticated techniques involved and the limited versatility of current platforms, methods of small animal radiation have yet to achieve the same quality as in clinical radiation therapy (Motomura et al., 2009). There is a limited number of published studies based on small animal irradiation and it may still take some time before the field uncovers its full potential (Verhaegen et al., 2011).

Recent developments of preclinical and small animal studies have been successful in answering the questions involved with human related health risks. The field of small animal irradiation has recently been emphasized by a group of scientists as they discussed the importance in the development of high precision micro-irradiators for the application based on small animal models (Verhaegen et al., 2011). Although the practice of irradiation may be similar to modern human radiotherapy process, the authors emphasized the use of kilovoltage energy beams with highly precise mounting and positioning systems to be practiced and used on research experiments involving small animals. Accuracy and precision is an important factor for the irradiation of specific targets within small animals. Beam delivery has to be controlled with sub-millimetre precision and as a result the authors have discouraged the use of megavoltage photon beams due to the extent of the dose build up region, which may go beyond the size of the small animal. The lateral penumbra from the megavoltage beams may extend several millimetres beyond the geometric field (Verhaegen et al., 2011). The recommended x-ray energy range suitable for small animal studies is between 100kVp to 300kVp.

Due to the advances in technology it is now possible to use radiotherapy approaches for research in areas other than cancer treatment. In particular the selective targeting of certain anatomical sub volumes in the brain of animal models is of interest in order to switch off certain functionality which in turn enables researchers to investigate the effects. These experiments have allowed the initiation of novel experiments to investigate the pathogenesis behind certain physiological dysfunction.

2.3 Rat Brain Anatomy

The hippocampus in a rodent brain is described as flat and elongated structure sitting between the medial part of the temporal lobe and underlying thalamus. In rats, the hippocampus extends caudally and ventrally from the dorsal midline just above the thalamus to the ventral subiculum (Sharma, 2007). The position of the hippocampus within the rodent brain is shown in figure 2.1.

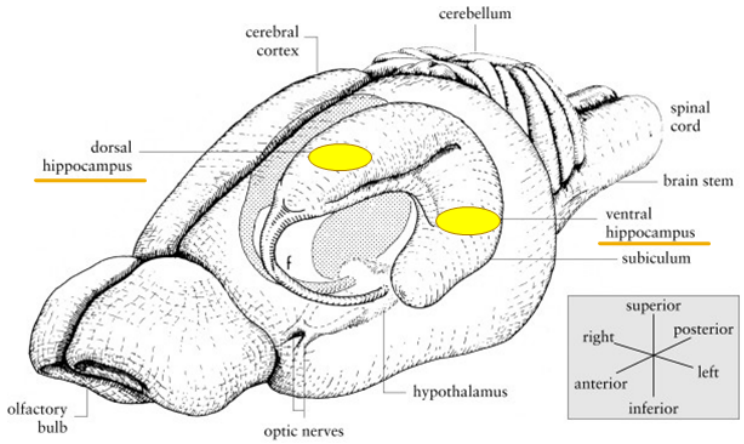

Figure 2.1: *Figure showing the rat brain and the hippocampus. The labelled areas show the dorsal and ventral hippocampus which will be targeted during the irradiation of the rat.*(Khoshnazar et al., 2012)

Anatomical landmarks such as bregma and lambda points on the skull and the midpoint of the interaural line are commonly used in stereotaxic surgery and radiotherapy. Figure 2.2 shows the bony structure of the rats head with the labelled positions of the bregma and lambda on the skull. It is possible to map the whole anatomy of the rat brain based on the

combination of these reference landmarks and this specific method is used to produce brain atlases or stereotaxic atlases dedicated to specific small animals. The stereotaxic atlases are based on a group of rats with equal properties such as weight, sex and strain (Paxinos et al., 1985). Studies have been performed to investigate the margin of errors that might exist due to the physical variability of the rat. It was reported that only marginal errors existed between the use of different sex and strain. However, significant errors in the position of the stereotaxic points were reported with the use of rats of varying weights. The position of the landmarks is an important parameter which needs to be fixed and constant for small animal irradiation which reinforces the importance of selecting the rats of the same age and weight.

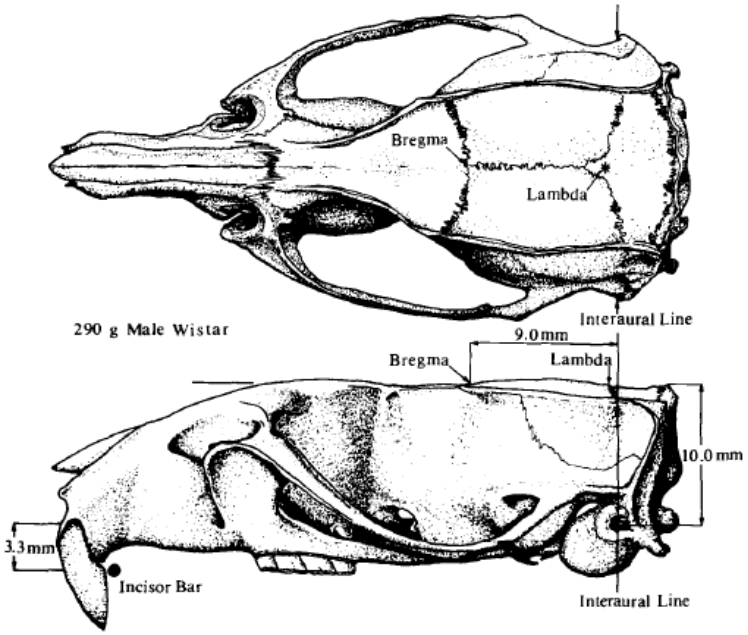

Figure 2.2: *Showing the anatomy of a 290g Male Wistar Rat. The landmarks on the skull are clearly labelled along with the distances. It has been shown that there are minimal differences in the position of the landmarks between the rats of the same weight.*(Paxinos et al., 1985)

2.4 Neurogenesis

Neurogenesis is a combination of process that includes cell division, migration and differentiation to generate functional neurons from neural precursors. The idea of neurogenesis in adult brains was traditionally viewed with resistance and was viewed to occur only during the embryonic and perinatal stages in mammals (il Ming & Song, 2011). However, from

the pioneering studies by John Altman decades ago proposed the first anatomical evidences of newly generated dentate granule cells in the postnatal rat hippocampus (Altman & Das, 1965).

Active adult neurogenesis is limited to two specific regions; subgranular and subventricular zone of the dentate gyrus. These areas are termed as neurogenic regions where new dentate granule cells and new neurons are generated repsecitvely. The newly generated neurons undergo a process termed as chain migration where it propagate through the rostral migratory stream towards the olfactory bulb to differentiate into interneurons (Leuner et al., 2006). Sequential steps of neurogenesis range form neural precursor proliferation to synaptic integration of newborn neurons (Gage et al., 2008). In reference to figure 2.3, the hippocampus is divided into three important sections; dentate gyrus, CA3 and CA1. The figure illustrates the steps involved in neurogenesis. The perforant pathway creates excitatory connections with the granule cells located in the dentate region of the hippocampus where the new neurons arise. The newborn cells and existing granule cells form a mossy fiber pathway projecting towards the CA3 pyramidal cells. The CA3 cells project towards the CA1 pyramidal cells via Schaffer collaterals. Neurogeneis in other regions is considered to be very limited under normal conditions (Deng et al., 2010).

2.5 Radiation Biology

Radiation biology is the study of the interaction between the ionizing radiation and living cells. It is a process which can be simply illustrated via the process of how the energy of the radiation is used to damage the cell‘s deoxyribonucleic acid (DNA). However, more in depth experimental research is still required to fulfil many of the unanswered questions that still exist in this study (Joiner & van der Kogel, 2009). The basic mechanism and the associated terminology have been provided to impart a clear understanding of the interaction with the living tissue, especially for health care workforce that utilizes ionizing radiation (Bolus, 2001). The pathway of the ionizing radiation interacting with living cells is classed as either direct or indirect interaction. In general the interaction of radiation with cells is a probability based function that is proportional to the total dose, exposure rate and type of cells due to the varying level of resistance.

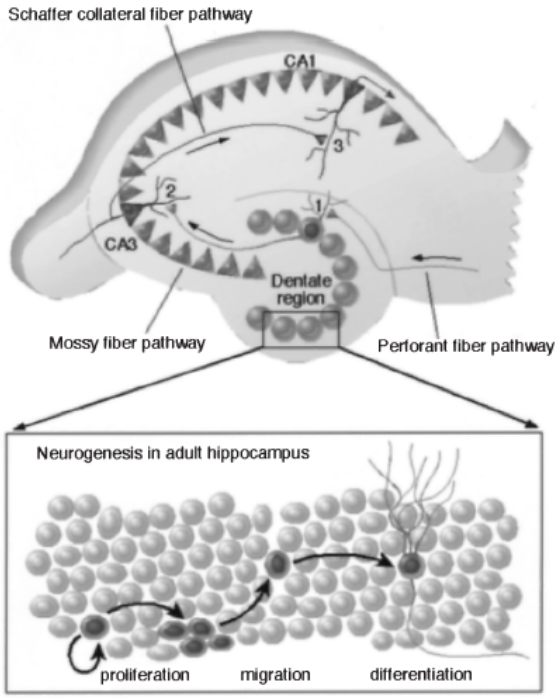

Figure 2.3: *Showing the proces of neurogenesis in adult rodent brain. It is a three step process; proliferation, migration and differentiation in the dentate gyrus of the hippocampus.* (Gage et al., 2008)

The interaction between the ionizing radiation and living cell is illustrated in figure 2.4. The direct interaction affects the cell as a whole by either killing the cell or mutating the base pairs within the double strand of the DNA. The aftermath of the mutation in the DNA results in permanent damage leading up to the breakage of the double stranded DNA structure and eventually to cell death. There is also a probability of the incoming radiation interacting with the cellular water molecules rather than the macromolecules within the cell. This results in an indirect interaction between the ionizing radiation with the living cells. The energy of the radiation is high enough for water molecules to undergo hydrolysis forming free radicals such as hydroxyl (OH-) within the cell. Hydrogen peroxide (H_2O_2) molecules are formed by the recombination two hydroxyl molecules which have toxic properties as they readily combines with organic compounds which can reduce the population of essential enzymes and eventually causing cellular death (Pordgorsak, 2005).

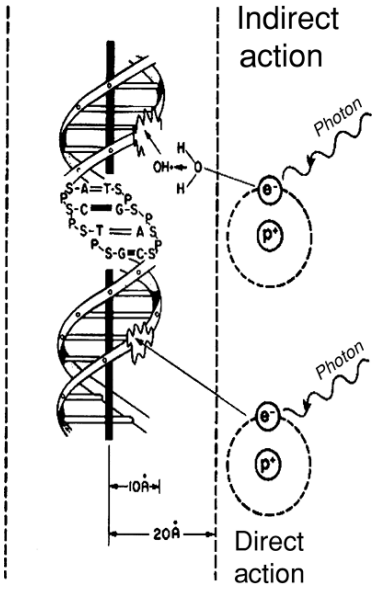

Figure 2.4: *Direct and indirect mechanism of the ionizing radiation interacting with the DNA. The ejected electrons by radiation can interact directly with base pairs of the DNA while indirect pathway utilizes the water molecules surrounding the DNA.*

2.6 Study of Radiation Induced Impairment of Hippocampal Neurogenesis

Ionizing radiation has become an essential tool in both medical imaging and treatment of cancer. However, the experimental uses of focal irradiation have expanded across various field and in particular studies of new neurons in the brain. It has recently emerged as the standard tool for animal studies on functional effects of adult neurogenesis (Snyder et al., 2005). Methods such as clinical linear accelerators (linacs) or micro-CT with dedicated small animal platforms have become common approaches to irradiate certain sub anatomical regions within the animal.

The effects of irradiation on the hippocampus have been a topic of interest as it is the primary region of neuronal progenitors which are associated with functions of memory and learning. There have been convincing evidences that the inhibition of adult neurogenesis in the dentate gyrus have significant effects in the memory that relates to past events (Tan et al., 2011). This non-invasive application of radiation delivering tools has proven to be successful in the study of common brain related diseases such as Huntington‘s disease and Alzheimer‘s disease. In addition, x-ray irradiation tools have been used to identify the pathogenic relationship of

cognitive deficits with reduced neurogenesis within the hippocampus. Although the mechanism of cognitive changes as a result of brain irradiation remains unclear, the pathogenesis of the post irradiation symptom can be associated with the reduction of neurogenesis within the hippocampus located in the medial temporal lobes (Rola et al., 2004). Focal irradiation techniques such as Gamma Knice (GK) (Schindler et al., 2011) and image guided radiotherapy (IGRT) techniques (Tan et al., 2011) have shown the effective reduction of the progenitor cells in the hippocampus and have achieved up to 80% suppression in the number cells. However, there have been mixed responses as some groups have reported that there have been no clear evidence in the results showing the impairment of hippocampus dependent test of spatial learning (Winocur et al., 2006). Due to the various outcomes, there still remain areas of further research using consistent neurogenesis depletion techniques and broader range of behavioural tasks are needed for a better understanding of adult neurogenesis in neurocognivitve function (Winocur et al., 2006).

2.7 Small Animal Irradiation Setups

The need for small animal related experiments have lead to the increase in demand of more radiation therapy technology dedicated for small animal irradiation (Woo & Nordal, 2006). There have been numerous publications relating to the development of research systems capable of precise irradiation of structures in small animals. Groups from Johns Hopkins University, Princess Margaret Hospital, Washington University, Stanford University and University of Texas Southwestern have either commenced modifications on existing technologies or have developed using their own resources. Two specific systems is reviewed in this thesis, developed from Johns Hopkins University and Standford University, to understand the level of specifications and engineering standard required for small animal irradiation applications.

Small Animal Radiation Research Platform (SARRP), shown in figure 2.5, is a collaboratively developed technology at the Johns Hopkins University. SARRP consists of an industrial 225kvp x-ray tube with dual focal spot (0.4mm and 3mm) which is used for both imaging and therapy. It is also equipped with the necessary tools for cone beam CT imaging guidance where the x-ray source and the flat panel silicon detector are fixed at positions of 90° and 270° respectively (Wong et al., 2008). The customized stage for the immobilization of the animal consists of a cylindrical tower mounted onto a robotic translation and rotational stage

with accuracy of 0.0065mm and 0.05° respectively. The combination of the rotating gantry and the multi dimension moblility of the robotic stage facilitates the delivery of complex conformal dose distributions (Wong et al., 2008).

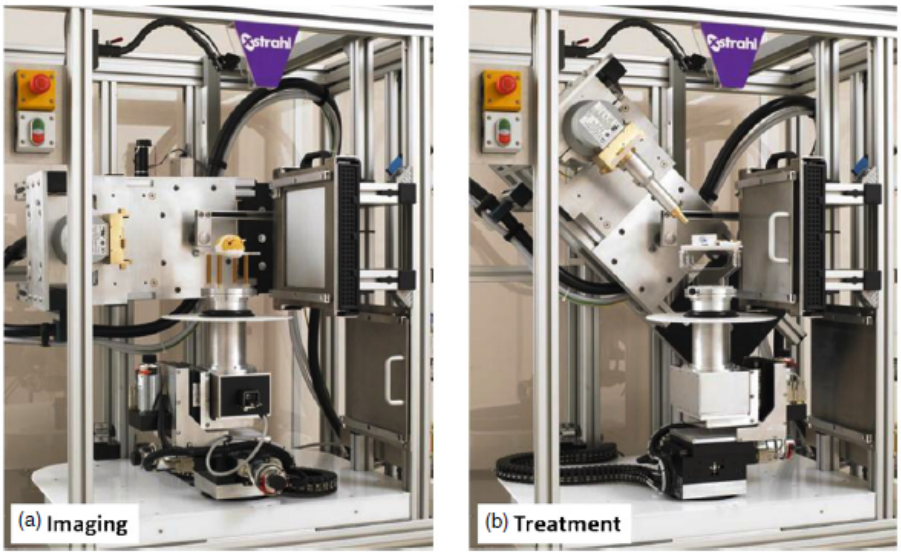

Figure 2.5: *Small Animal Irradiation Research Platform (SARRP) developed at Johns Hopkins University.*(Matinfar et al., 2009)

In contrast to SARRP, a team at the Department of Radiation Oncology at Standford University have built and developed on an existing commercial micro-CT scanner. GE eXplore RS120 microCT scanner has been modified by integrating a x-y translational stage along with a variable aperture collimator (Zhou et al., 2010). The modified setup is shown in figure 2.6. The collimator is one of the unique features of this specific system as it consists of 12 pentagonal lead-brass blocks arranged in two planes for two stage collimation. The collimation can produce pseudo-circular field sizes of between 1mm to 102mm at the CT isocentre. The microCT system operates at 120kVp with a max current limit of 50mA and the rotating gantry can be used for irradiating animals in either arc-fashion or from specific angular directions.

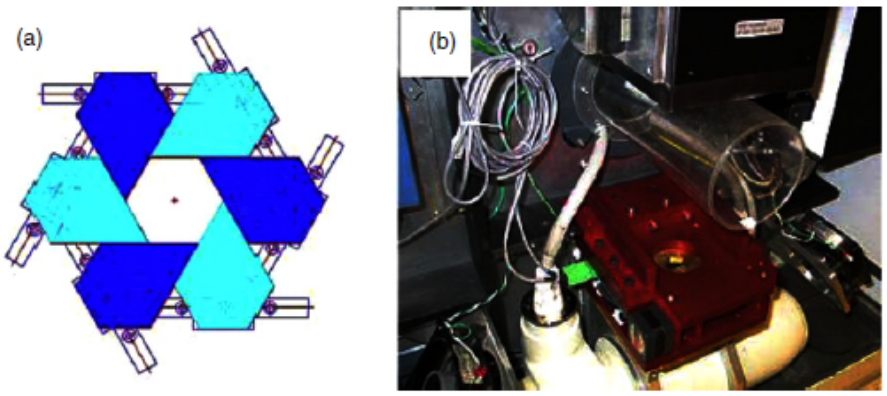

Figure 2.6: *The micro-CT scanner modified by Stanford University to be used for small animal irradiation related studies. (a) shows the mechanical hexagonal collimator (b) the micro CT modified for small animal studies*(Rodriguez et al., 2009)

CHAPTER 3

Methods and Materials

This chapter describes the methods and materials that were used during the project. The project consisted of numerous experiments involving radiation dosimetry, designing of a live rat holder and preparation of the rats prior to irradiation. The chapter briefly overviews the functions behind the materials and equipments used with the basic theory where it is needed.

3.1 MARS Spectral CT

MARS spectral CT is a micro CT scanner developed by the MARS group in the Department of Physics and Astronomy, University of Canterbury. The scanner, initially built for producing coloured CT images, has aspects which can be further utilized and progressed towards the platform of image guided radiotherapy for live small animals. The Mars Spectral CT system is a desktop x-ray scanner consisting of a micro focus x-ray tube aligned with a photon counting detector, Medipix camera, for imaging. The setup consists of a rotating gantry mechanically controlled by a motorized system. It is designed to image small specimens of up to 100mm diameter and 300mm length (Zainon et al., 2010). Maximum x-ray tube voltage depends on the version and the model number scanner ranging from unit-1 to unit-10. The maximum tube voltage .

The scanner used for irradiation was the MARS version 4 scanners, either unit 6 or unit 8,

Figure 3.1: *MARS spectral CT located on the 4th floor Department of Physics and Astronomy. The shown scanner is the MARS-unit6, a version 4 scanner integrated with the 120kVp x-ray tube.*

integrated with the 120kVp x-ray tube. Due to the fact that most kilovoltage x-ray delivers a high skin dose, the scanners with the highest available tube voltage was used to minimize the x-ray attenuation from the skin. The value is also supported through literatures, mentioned in the previous chapter, as the recommended range for small irradiation is between 100kVp and 300kVp.

3.2 Live Rat Holder

Prior to the irradiation it was decided that a new setup was needed to place live anaesthetized rats inside the scanner for irradiation. Thus a holder was designed and built with the appropriate parameters and specifications to reliably position the rats inside the machine. Stability and precision were considered as the main traits when designing the holder as it was important to minimize any margin of variation in positioning of each individual rat. Due to the fixed position of the lead collimators, the constant position of the rat maintains the specific area of the brain irradiated consistent.

The original holder was constructed with a circular base and an elevated platform to rest and elevate the head of the rat. However due to instability of the setup the holder was redesigned and rebuilt as shown in figure 3.2. The modified holder consists of a rectangular base and stereotaxic surgery bars that were integrated to improve the method of fixing the rats head in a constant position. The stereotaxic surgery system is a three piece bar consisting of two ear bars and a nose bar is used to fixate the rats head for the surgical procedure performed on the brain.

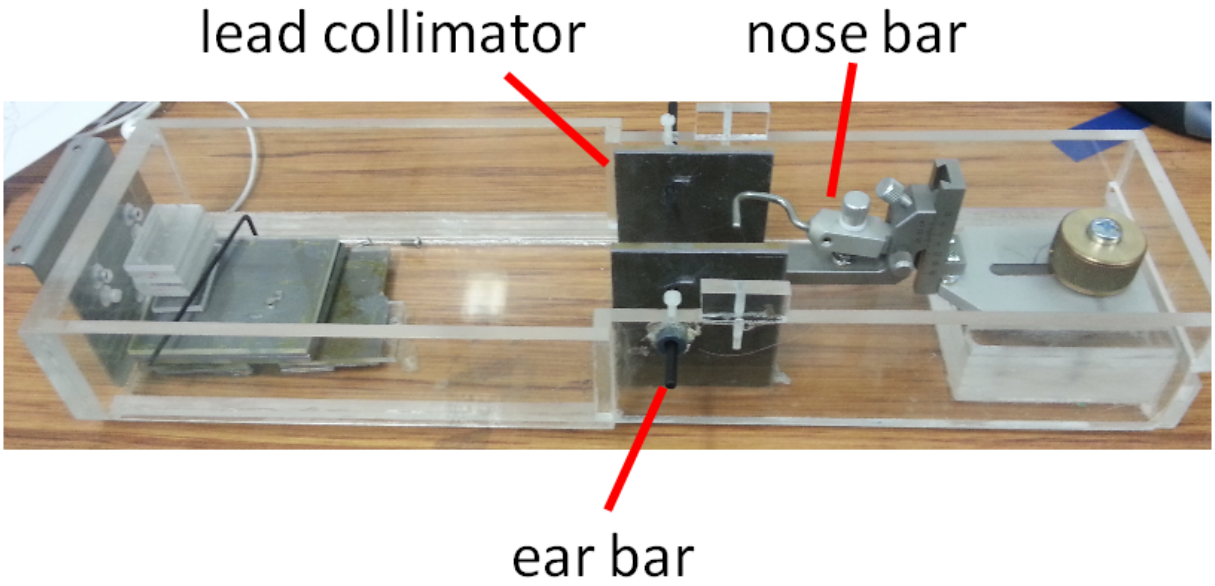

Figure 3.2: *Showing the apparatus for specifically desgined to place a live rat inside the MARS CT machine for irradiation. It consists of two ear bars and an adjustable nose bar and also the lead collimators.*

3.3 Ionization Chamber

Ionization chambers are gas filled detectors that are commonly used for radiation dosimetry. The gas in the chamber form charges as a result of direct ionization and are collected through the application of an electric field. One of the advantages of using ionization chambers is the uniformity of the radiation response over a wide range of radiation energies and is a preferred tool for most calibration and quality assurance assessments in clinical departments.

The main principle of ion chamber operation based on measuring of the charge proportional

to the number of ion pairs created in the gas. Gas filled chamber consists of two electrodes; anode and cathode. The incident ionizing radiation creates positive ions and electrons where they are directed towards the electrodes of the opposite polarity under the influence of the electric field. The accumulated charge on each electrode is proportional to the number of ion pairs created which also is proportional to the radiation dose. The continuous generation of ion charge creates an ionization current which is measured by through an electrometer circuit shown by figure 3.3.

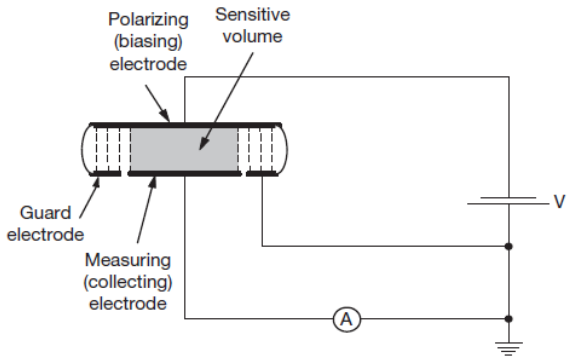

Figure 3.3: *The mechanism of the ionization chamber. The sensitive area corresponds to the chamber filled with gas for ionization. The current from the electrodes are proprotional to the ionizing radiation dose*

The ion chamber developed by Unfors RaySafe® was used to measure the x-ray dose rate inside the MARS scanner. The physical apparatus of the equipment is shown in figure 3.4. The ion chamber, RaySafe® Xi, is a hybrid ion chamber combined with an electronic readout meter connected via USB cable. One of the unique advantages of using this specific dosimeter is the minimal requirement of correction factors due to the automated post readout correction process. The equipment was obtained from Canterbury District Health Board with the assistance of an accredited medical physicist.

3.4 Films

In addition to the ion chamber, film dosimetry was also used measure the depth dose characteristics of the kilovoltage x-rays. Films have specific advantages over ion chambers such as high spatial resolution and the ease of use to measure the depth dose distribution. In partic-

Figure 3.4: *Raysafe® Xi. The ionization chamber is connected to the readout via usb. The chamber is of compact size for durability a*

ular, Gafchromic® films have become more commonly used in clinical departments and have replaced original radiochromic films which were based on cyanide dye. The Gafchromic® film consists of thin microcrystalline sensitive layer coated on a flexible polyester film base and has equivalent chemical properties of living tissue. The film can be cut into any dimension and shape, ideal for the meticulous knowledge of isodose curves and depth dose curves. The orange polyester base progressively turns blue upon radiation exposure as the amount of bluing is proportional to the absorbed dose of the ionizing radiation.

The Gafchromic® XR-QA was used to measure the x-ray exposure at different depths of Perspex. The film was calibrated using the Raysafe® Xi ion chamber to initially understand the characteristics and appropriate range of the radiation dose the film can be exposed to ("Gafchromic XR-QA Dosimetry Film Product Brief", n.d.). Calibration procedure involved exposing the Gafchromic® XR-QA with the known dose measured using the hybrid ion chamber. The film and its chemical composition is shown in figure 3.5 where the polyester layer has tissue equivalent properties and the active layer is the source of the radiation induced blue dye. The specifications of the film is also shown in the list.

Figure 3.5: *Showing a sheet of the Gafchromic® XR-QA. The chemical composition of the film and thickness is shown by the figure on the right*

- Dose range: 0.1cGy to 20cGy
- Energy range: 20kVp to 200kVp
- Size: 10inch x 12inch
- Configuration: 3-layer (laminate substrate - active layer - substrate)
- Substrate: Clear polyester (97 microns)
- Active layer thickness: 25 microns

3.5 Perspex Phantom

Perspex sheets were used to provide depth due to its water equivalent properties to mimic the physical layers of tissue. Figure 3.6 shows the Perspex phantom where individual pieces of Gafchromic® film can be placed between different layers to produce a depth dose curve. Table 3.1 shows the thickness of the individual pieces of the labelled Perspex in the figure measured using an electronic micrometer.

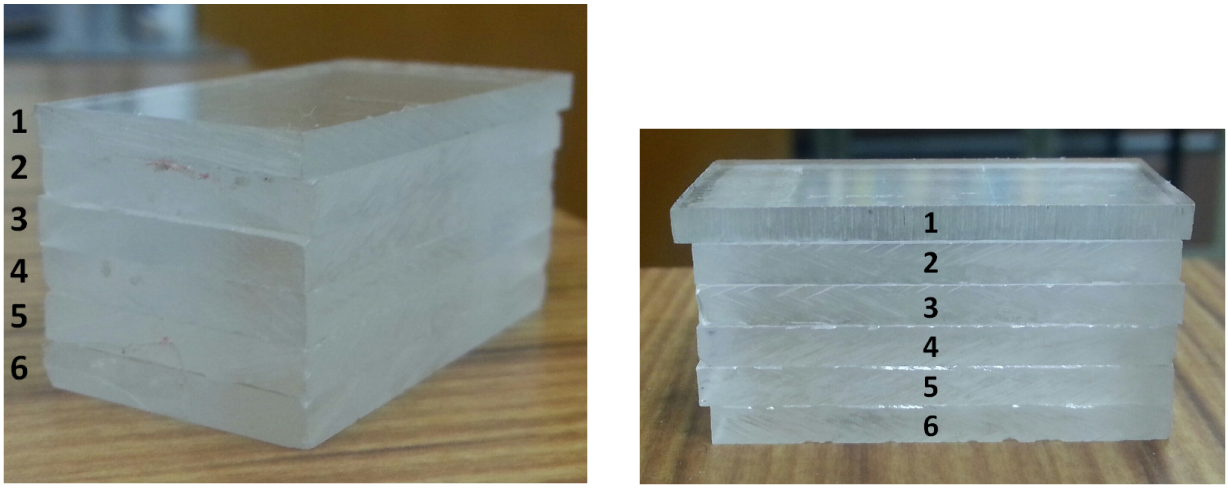

Figure 3.6: *Showing the phantom of multiple layer of persex sheets. The phantom can easily be adjusted to insert Gafchromic® films between each layer to obtain a depth dose curve*

Perspex no.	thickness (mm)
1	2.68
2	3.15
3	3.10
4	3.15
5	3.12
6	3.13

Table 3.1: *Table showing the estimated values of the x-ray dose at different depths of Perspex measured using the Gafchromic® XR-QA*

3.6 Preparation of the Rats

Long Evans rat at an age of four weeks were prepared by the Department of Psychology, University of Canterbury. The specific breed and size of the rats were used irradiation of the brain and also for imaging experiments using the x-ray projections. Prior to the irradiation, the rats were administered with 5-bromo-2-deoxyuridine (BrdU) which is a synthetic thymidine analog that gets incorporated in to a cell when it is dividing. The BrdU has been used by numerous groups seen in literatures to provide a visual evidence of the cell division within the hippocampus. The BrdU was dissolved in phosphate-buffered saline (PBS) for a final concentration of BrdU 25 mg/ml. The solution was injected at a dose of 200mg/kg to the rats as this was performed twice, 24 hours and 4 hours before irradiation, to improve the efficiency in the labelling of the neurons in the hippocampus.

Doublecortin (DCX) immunohistochemistry was also used as an alternative method of staining to be compared with the BrdU. DCX is progenitor neural cell marker, a microtubule associated phosphor-protein, which are also used for analyzing alterations in neurogenesis in the adult dentate gyrus (Park et al., 2012). The unique features of the DCX is its ability to quantify both number and the dendritic growth of the new neurons which can be useful in evaluating the change in the hippocampal neurogenesis as a function of neurodegenerative diseases (Park et al., 2012)

3.7 Irradiation

Parallel opposing beam was used to irradiate the hippocampus. Figure 3.7 shows the geometrical setup of the x-ray source relative to the position of the rat and the lead collimators. The lead collimators were used to confine the cone beam of the x-ray and minimize the radiation exposure to non-target regions within the brain. The diagram illustrates how the conformal shaping of the cone beam x-ray is achieved using lead collimators.

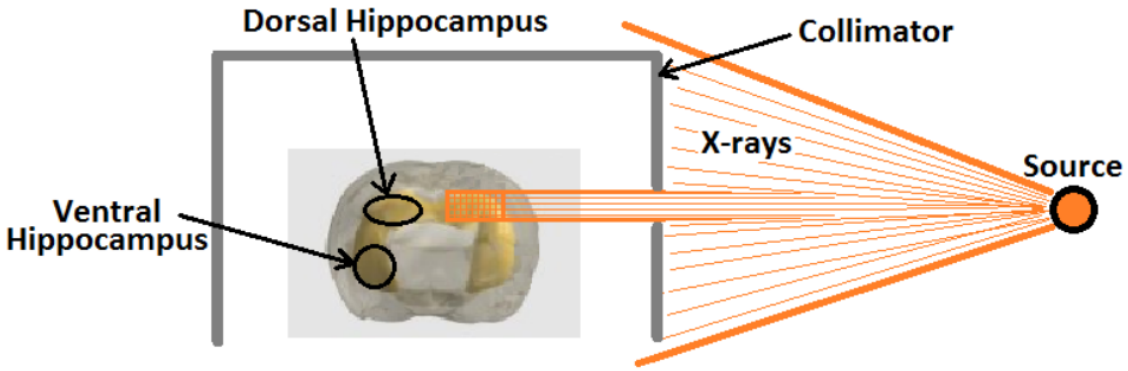

Figure 3.7: *Diagram showing the basic setup for the rat irradiation inside the scanner. Parallel opposing beam geometry is used where the x-ray is rotated 180 degrees to irradiate the opposite lateral side.*

CHAPTER 4

Radiation Dosimetry

This chapter focuses on the procedures performed to measure the radiation delivered from the x-ray source inside the MARS Spectral CT. The chapter describes the measurements made using ion chamber and radiochromic films to understand the characteristics of the kilovoltage x-ray beam. Perspex material was used with the radiochromic films to produce depth dose curve.

4.1 Dosimtery

Radiation dosimetry is a standard procedure in evaluating the physical quantity and quality of the ionizing radiation. One of the primary roles is to measure the level of absorbed dose in matter and living tissue as a result of both direct and indirect exposures. Our understanding of ionizing radiation and the pathways of damaging living cells has increased due to the experiences gained through industrial and clinical application and also via radiation related mistakes and tragedies. As a result, protocols and standards are established by international and national agencies to maintain the safety of radiation usage by providing local rules and guidelines for dosimetric procedures. In particular, national bodies such as the American Association of Physics and Medicine (AAPM) and National Radiation Laboratory (NRL) are one of many national bodies providing annual reports, dosimetry guidelines and also calibration of radiation monitoring equipments (Ma et al., 2001) (McEwan, 2004).

4.2 X-ray Production

The x-ray tube, shown in figure 4.1, is the standard method of producing x-rays used for medical purposes. The tube consists of a vacuum with heated filaments which emit electrons through a process known as thermionic emission. High voltage source is applied to accelerate the electrons towards the anode, labelled as A in the figure, which commonly is a metal target with a high atomic number such as tungsten. The electrons become subject to inelastic interactions with the atomic nuclei due to the coulombic force between the electron charge and positively charged nucleus. The path of the electron is deflected resulting in a loss of kinetic energy causing instantaneous emission of x-ray radiation commonly called as bremsstrahlung, German word for describing braking radiation (Bushberg et al., 2006).

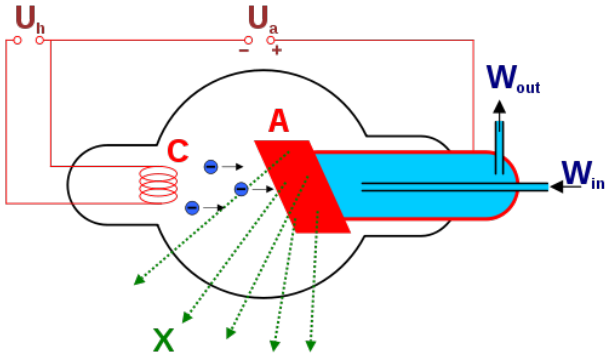

Figure 4.1: *Basic diagram of the x-ray tube and the concept of how the x-rays are produced and emitted. (A) corresponds to the target anode while (C) is the heated filament for releasing electrons.*

The probability of bremsstrahlung production increases with the energy of the incoming charged particle and the atomic mass of the target material (Jevremovic, 2009). The relationship is represented through equation 4.1 where the ratio of the electron energy loss by bremsstrahlung is calculated from the atomic number of the anode, Z, and kinetic energy of the incident electron, E_k. The output energy of the bremsstrahlung radiation consists of a continuous spectrum ranging up to and including the entire energy of the deflected electrons. This process of radiative energy loss is the primary method of producing x-rays used clinically and for research.

$$\frac{BremsstrahlungRadiation}{ExcitationandIonization} = \frac{E_k Z}{820} \tag{4.1}$$

4.3 Measurement using Ionization Chamber

The Raysafe®-Xi ionization chamber was used to measure the x-ray output inside the MARS Spectral CT. The ionization chamber was placed at the centre of rotation of the gantry with an approximate source to detector distance of 140mm. Table 4.1 shows the x-ray dose measured at the maximum tube voltage of 120kVp at varying current settings from 0uA to 350uA. For each current value, the ion chamber was exposed to the x-ray for 60 seconds. The plot showing the linear relationship of the x-ray tube current and the measured dose is shown in figure 4.2. The maximum dose rate of the x-ray tube inside the MARS Spectral CT measured using the ion chamber was 529.6mGy.

Current (uA)	Dose (mGy)
0	0
17.5	27.5
35	57.2
70	106.1
105	159.7
140	211.6
175	264.6
210	319.2
245	373.9
280	423.6
315	477.6
350	529.6

Table 4.1: *Table showing the dose measure using the Raysafe®-Xi ionization chamber at different x-ray current settings.*

4.4 Film Calibration

To be able to quantify the amount of radiation dose absorbed by the radiochromic films, the films were calibrated with the known x-ray exposures measured from the ionization chamber. Thus identical setup and procedure was used to ensure equal amount of radiation dose was delivered to the film. The Gafchromic® XR-QA film was cut into multiple pieces of smaller

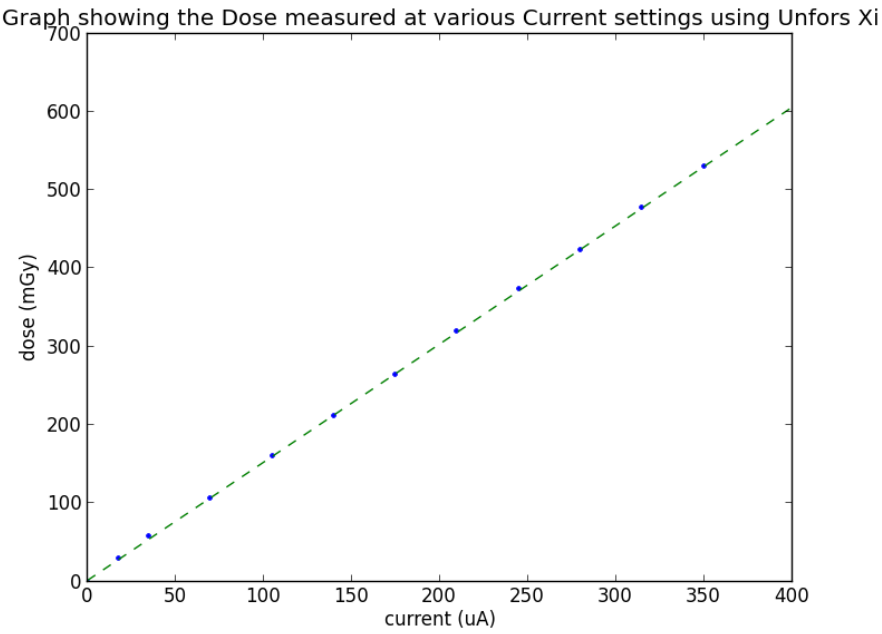

Figure 4.2: *Graph showing the dose measured using Raysafe®-Xi at various current settings on MARS CT-6 at 120kVp*

dimensions, as shown in figure 4.3, where each of the films were exposed to the x-ray at different current settings. The darkening of the film progressively becomes more significant at higher current values and it is the amount of this darkening that is used to correlate with the absorbed radiation of the film and produce a calibration graph.

To analyse the films, the films were converted into a digital image. The exposed films were scanned using a flatbed scanner, Ricoh Alficio MP5000, set at greylevel setting of 400 dots per inch (dpi). The pieces of the film were consistently scanned in the landscape orientation due to the reported variation in the optical density with scanning orientation (Gould & Gross, 2002). Film analysis was performed using the image analysis software, ImageJ, which has the tools to measure the mean greylevel values on the exposed area of the film. The analysis step is illustrated in figure 4.4 where the yellow box specifies the area within the exposed region of the film that was used to measure the mean greylevel. The greylevel values for each x-ray current settings is shown in table 4.2. The mean greylevel values were converted into optical density values using equation 4.2. Equation 4.2 is a logarithmic function of the relative value between the mean greylevel of the unexposed film, I_o, over the mean greylevel value of the exposed film, I. The optical density along with its equivalent

measured radiation dose was used to produce the film characteristic curve shown in figure 4.5.

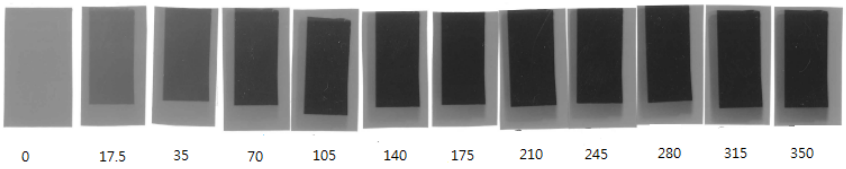

Figure 4.3: *Figure showing pieces ofGafchromic® XR-QA exposed to x-ray at a range of different current settings from 0uA to 350uA*

Figure 4.4: *Figure showing a single piece of Gafchromic® XR-QA for analysis. The yellow box is used to specify a region of area in the exposed section to measure the mean greylevel using ImageJ*

$$O.D. = \log \frac{I_o}{I} \tag{4.2}$$

Current (uA)	Dose (mGy)	Mean grey value
0	0	154.89
17.5	27.5	116.11
35	57.2	94.68
70	106.1	66.76
105	159.7	56.02
140	211.6	43.67
175	264.6	37.39
210	319.2	35.55
245	373.9	34.27
280	423.6	29.83
315	477.6	29.21
350	529.6	27.43

Table 4.2: *Table showing the dose measure using the Raysafe® -Xi ionization chamber at different x-ray current settings. The table also includes the mean grey value measured on the exposed Gafchromic ® XR-QA film.*

The characteristic curve of the film is divided into two specific regions, the linear portion and the shoulder region. To measure the absorbed dose using films, the range of the x-ray exposures applied to the film should always lie on the linear portion of the film‘s characteristic curve (Pordgorsak, 2005). In reference to figure 4.5, the shoulder region of 200mGy specifies the upper limit of the dose range, where beyond this point the optical density reaches a threshold value and unable to differentiate between the absorbed dose. As a result when performing dose measurements using the Gafchromic® XR-QA, the x-ray from the MARS CT was always set at a low current setting of 70uA to maintain the exposure within the limited range of the film. The absorbed doses at higher current values were numerically calculated from the linear relationship between the x-ray current and the absorbed dose.

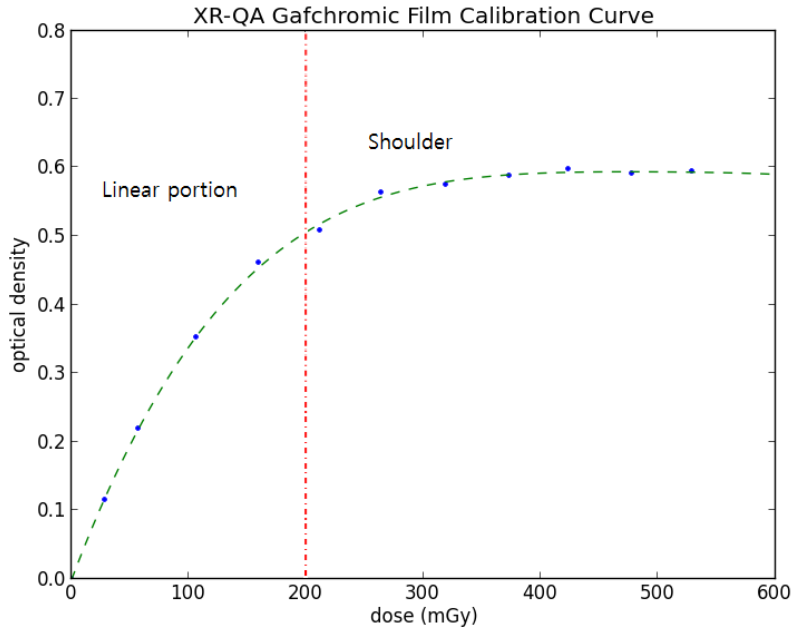

Figure 4.5: *Graph showing the Gafchromic ® XR-QA characteristics curve. The curve is split into two regions; linear and shoulder. Measurements with Gafchromic films should always be performed within the linear region.*

4.5 Depth Dose

One of the main advantages of film dosimetry is the ability to measure the depth dose characteristics of the incident radiation. Perspex sheets were used to analyse the depth dose characteristics of the x-ray inside the MARS Spectral CT. The phantom shown in figure 3.6, Chapter 3, was used to simulate the depth properties as the Gafchromic® XR-QA films were inserted between the different layers of the Perspex sheets. Table 4.3 shows the optical density of the films irradiated at different depths of Perspex. The absorbed dose was calculated using the film characteristic curve, figure 4.5, where a polynomial fit was used to correlate between the optical density and dose. The depth dose plot is shown in figure 4.6 where the data was fitted with an exponential function shown by the red curve. The exponential function was used to estimate the point dose delivered to the hippocampus in the rat brain by measuring the depth using radiographic images which will be shown in Chapter 5.

$$dose = 66.837 \times \exp^{-0.059 \times x} \tag{4.3}$$

Depth (mm)	Optical Denisty	Dose (mGy)
0	0.23453	68.3580
2.68	0.18946	55.8494
5.83	0.1722	46.5296
8.93	0.15688	39.7647
12.08	0.1325	33.2890
15.2	0.1111	26.9106

Table 4.3: *Table showing the calculated values of the x-ray dose using the optical density of the exposed Gafchromic® XR-QA and its calibration curve.*

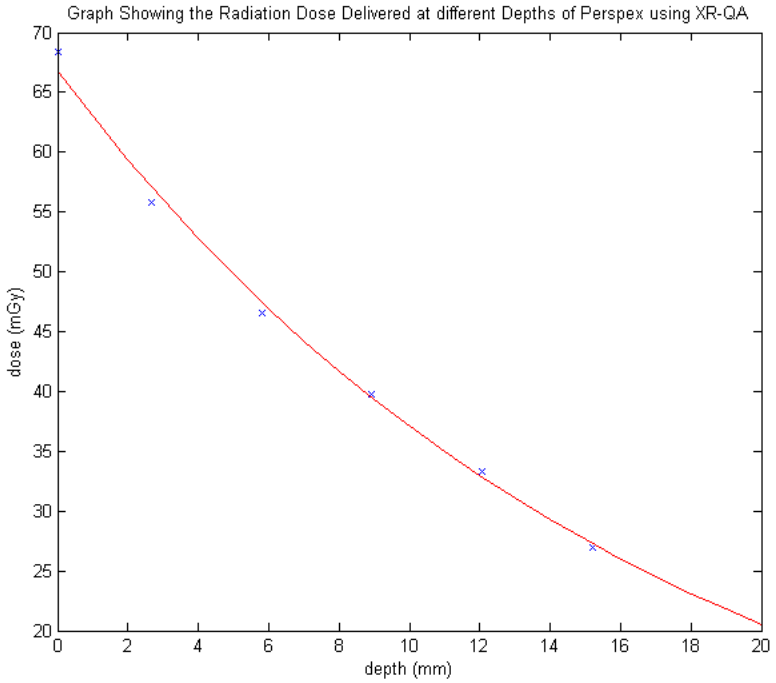

Figure 4.6: *Graph showing the depth dose curve. This was obtained by fitting an exponential fit to the data obtained by measuring the radiation at different depths of Perspex usingGafchromic® XR-QA.*

CHAPTER 5

X-ray Imaging of Rats

This chapter introduces x-ray imaging and how it arises through the different photon atomic ineractions. The chapter includes radiographic images of a euthanized rat illustrating the location of the bony landmarks and how it is used to locate the dorsal and ventral area of the hippocampuses within the brain. A recently developed function in the MARS CT, Preview Mode, is introduced with a script round process of the image formation and post processing method used to improve the image quality.

5.1 X-ray Imaging

X-ray imaging is the process of the x-ray photons penetrating through the object‘s body and projecting the shadow image onto an image receptor. The visibility and contrast in x-ray imaging involve multiple factors ranging from anatomical environment, image receptor quality and image processing. However the basic source of contrast in anatomical x-ray imaging originates from the differences in the physical density and the atomic number between the various anatomical structures within the body. Different densities result in varying rate of attenuation of the x-ray beam as it propagates through the body. The relationship between the x-ray transmission and the attenuation coefficient of materials, u, is shown through the Beer Lamber law, equation 5.1.

$$I = I_o e^{\mu x} \tag{5.1}$$

The linear attenuation coefficient of materials are dependent on the x-ray energy and the atomic number of the element composing the material. The difference in the atomic number from that of the surrounding tissue contributes to image contrast. Images are formed from the varying rate of x-ray transmission through object and to the image receptors where the remaining intensities of the x-ray is absorbed and processed. Images receptors range from radiographic films to photon counting detectors such as the Medipix detectors. Radiographic films are composed of sliver halides that turn dark upon x-ray exposure resulting in brighter region in the areas of soft tissue compared to bone. In contrast, the areas of high exposure in photon counting detectors will be brighter compared to the areas of low exposures. This difference is seen through the figures in the later sections of this chapter.

The x-rays consist of high energy photons which can ionize and disrupt the molecular bonds of objects. The interactions between the x-ray and the atoms in the object can be divided into three different categories; photoelectric absorption, Compton scattering and Rayleigh scattering. The degree and the probability of each interaction depend on the elemental composition of the imaging sample and also the energy of the emitted x-ray. For materials such as bones with high atomic number and density, the predominance of the photoelectric effect is what makes them clearly visible in radiographic images. For higher x-ray energies Compton scattering is the dominant interaction between soft tissue and x-rays, and is the primary source of soft tissue contrast.

5.1.1 Rayleigh Scattering

Rayleigh scattering, shown in figure 5.1, is a process of elastic interaction between the x-ray photon and the atom. It mainly occurs at the low end of the diagnostic energy range of between 15 to 30 keV. The interaction begins by the electromagnetic wave of the x-ray photon exciting the atom causing it to oscillate in phase (Bushberg et al., 2006). The energy of the incident x-ray is absorbed by the electron cloud and radiated at a different direction but with the same energy. The probability of Rayleigh scattering affecting image quality is very rare in most medical imaging applications. In soft tissue, Rayleigh scattering accounts for less than 5% of x-ray interactions above 70keV (Bushberg et al., 2006). However the interaction

needs to be considered for application such as mammography which uses very low diagnostic x-ray energies.

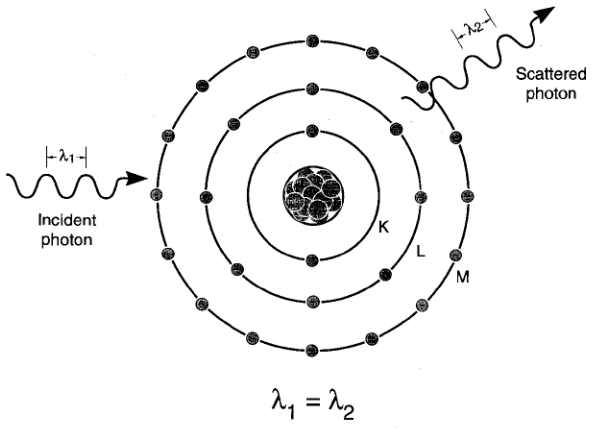

Figure 5.1: *Diagram illustrating the photon interaction of Rayleigh scattering. The scattered photon has the same energy as the incident photon. (Bushberg et al., 2006)*

5.1.2 Photoelectric Absorption

Photoelectric absorption is a process which the incident photons are absorbed by the orbital electrons of the atom. The absorbed energy results in ionization of the atom by the emission of electrons known as photoelectrons and this is illustrated in figure 5.2. The vacant position is filled by the electrons located at the lower binding energy shells producing characteristic x-rays and Auger electrons which are absorbed locally. The maximum kinetic energy of photoelectrons is calculated from the theory of energy conservation, equation 5.2. The kinetic energy of the electron, K_{max} is the remaining energy from the incident photon energy, hv, which loses energy from the releasing of the electron from its shell binding energy, E_b.

$$K_{max} = hv - \varphi \tag{5.2}$$

The photoelectric effect is the predominant process of x-ray interactions at lower energies. The interaction is also subject to statistical process and the probability of the photoelectric absorption is approximated from the cross section of the interaction, ϕ, shown in equation 5.3 (Davisson, 1965).

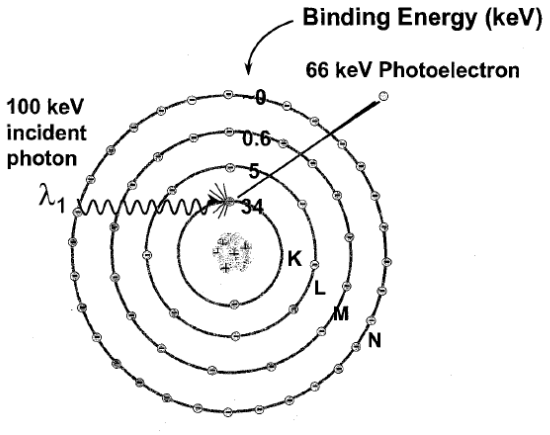

Figure 5.2: *Photoelectric absorption showing a 100keV photon interacting with an iodine atom. (Bushberg et al., 2006)*

$$\phi = \frac{Z^{4-5}}{E^3} \tag{5.3}$$

The equation shows that the probability of the photoelectric effect has a very strong relationship to the atomic number, Z, and photon energy, E. The probability is proportional to the Z^{4-5} representing the amplified absorption of the photons occurring in the bone relative to soft tissue. The contrast between the tissue is also dependent on the x-ray energy as it is inversely proportional to the E^3. This infers that the photoelectric effect is the main x-ray atomic interaction in the low energy ranges and is the predominant process for contrast between bone and tissue in radiographs (Khan, 2003).

5.1.3 Compton Scattering

Compton scattering, shown in figure 5.3, is the predominant photon interaction with soft tissue within the diagnostic energy range of 20keV to 150keV. The interaction results in ionization of the atom as the incoming x-ray is scattered by the outer shell electron which is ejected and referred as recoil or compton electron. The kinetic energy of the compton electron is lost due to the additional ionization it causes to the surrounding atoms. The energy of the scattered photon is calculated from the deflection angle of the scattered photon, ϕ, and the energy of the incoming x-ray, E_0, by using the Klein-Nishina Formula shown in equation 5.4.

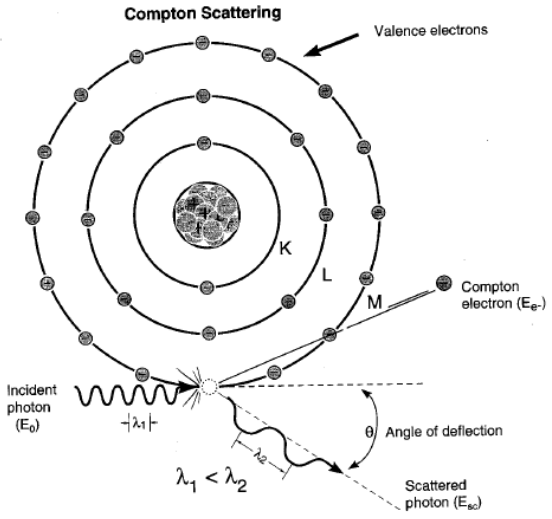

Figure 5.3: *Compton scattering diagram. The incident photon energy is used to release the compton electron and the remaining photon energy is scattered at angle of ϕ. (Bushberg et al., 2006)*

$$E_{sc} = \frac{E_o}{1 + \frac{E_o}{511keV}(1 - cos\phi)} \tag{5.4}$$

In contrast to the photoelectric absorption, the probability of occurrence of Compton scattering is dependent on the electron density of the absorber (Khan, 2003). The probability also increases with the incident x-ray energy due to the electron binding energy which is the minimum energy required for the effect to take place. The scattered photons are detectable via image receptors which reduces the primary photon attenuation differences between tissues. This results in degradation of the x-ray image.

5.2 Anatomical Landmarks in the Rat Brain

Anatomical landmarks are defined as specific areas in the anatomy that can be used as a point of origin to locate other anatomical structures. In addition to external fiducial markers, the use of landmarks for targeting is a common technique in radiation oncology in which electronic portal images are used to verify the patient position and radiation field placement. For the irradiation of the rat‘s hippocampus, a combination of bony landmarks were used as reference points. The combination of bregma and lambda points located on the skull and the interaural line is commonly used as reference points for stereotaxic surgery. Simple averaging

of the co-ordinates within the multiple reference point system is proven to be more than adequate when locating structures in the brains of rats (Paxinos et al., 1985).

The shapes shown by the plots in figure 5.4 represent the areas of the dorsal and ventral hippocampus in relation to the position of the bregma point and the mid point of the interaural line. The x and y axis of the plot corresponds to the distance above the interaural line and posterior to the bregma point respectively. The shapes on the figures were drawn using a rat brain atlas, The Rat Brain in Stereotaxic Coordiantes (Paxinos & Watson, 1997). The atlas is based on the combination of reference points such as bregma and the interaural line and also assuming that the top surface of the skull in a flat orientation. The atlas is successfully used for rats weighing between 250g and 350g (Paxinos et al., 1985). The figures were used as a reference map to locate the dorsal and ventral hippocampus in radiographic images of the rat and also for the design of the external lead collimators.

The series of radiographic images shown in figure 5.5 were taken at the Department of Radiology at Christchurch Women‘s Hospital. The radiographic images of euthanized rats were analyzed to locate the areas of the hippocampus using the anatomical reference points. To visualize the position of the landmarks, surgical pins, composed of stainless steel, were placed in both bregma and lambda positions on the skull. The steel pins show a bright signal in the image due to the high attenuation coefficient of the steel pin relative to the anatomy. The radiographs were viewed through a viewing software dedicated for radiographs at the hospital in which the reference lines and area plots were added to locate the dorsal area of the hippocampus. The green lines are used to mark the distance from the reference points and the yellow line specifies the area of the hippocampus. The lines are in scale and were drawn using the coordinates shown in figure 5.4.

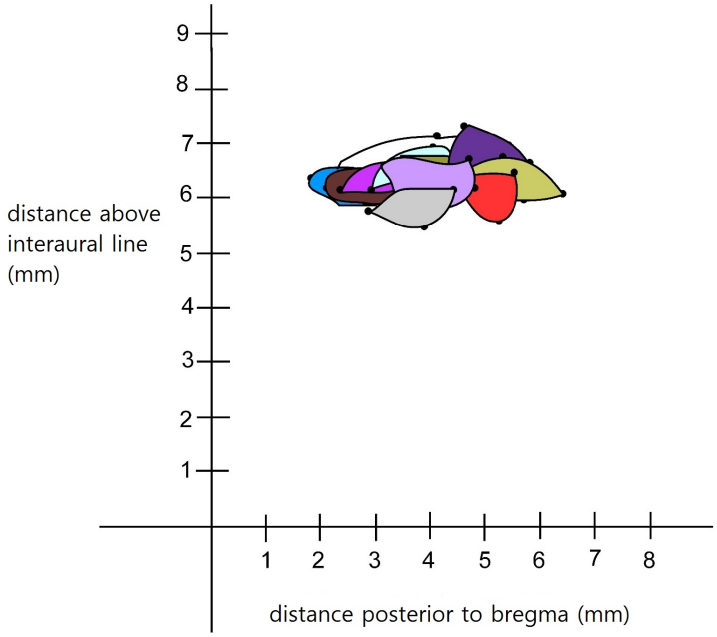

(a) Dorsal

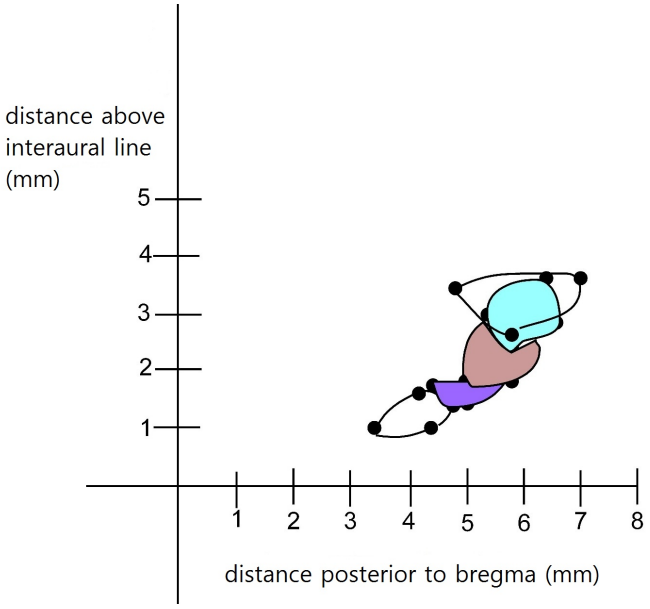

(b) Ventral

Figure 5.4: *Plots showing the areas of the dorsal (a) and ventral (b) hippocampus relative to the position of the bregma and the interaural line.*

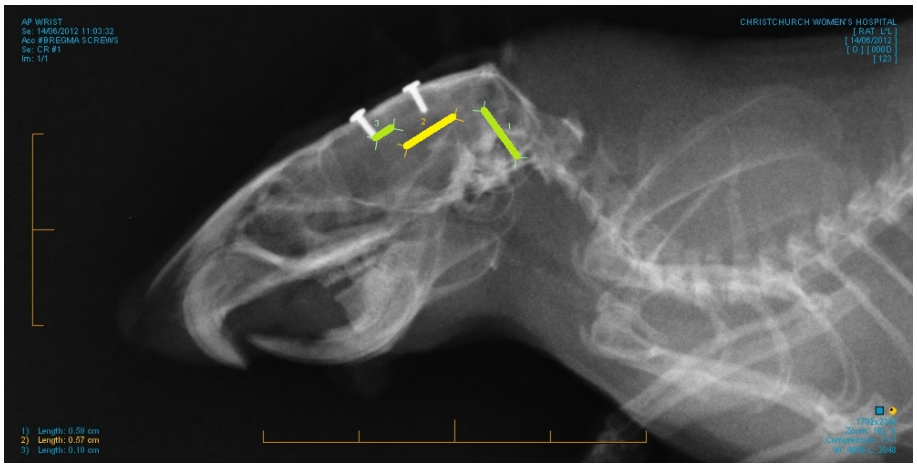

(a) Lateral view

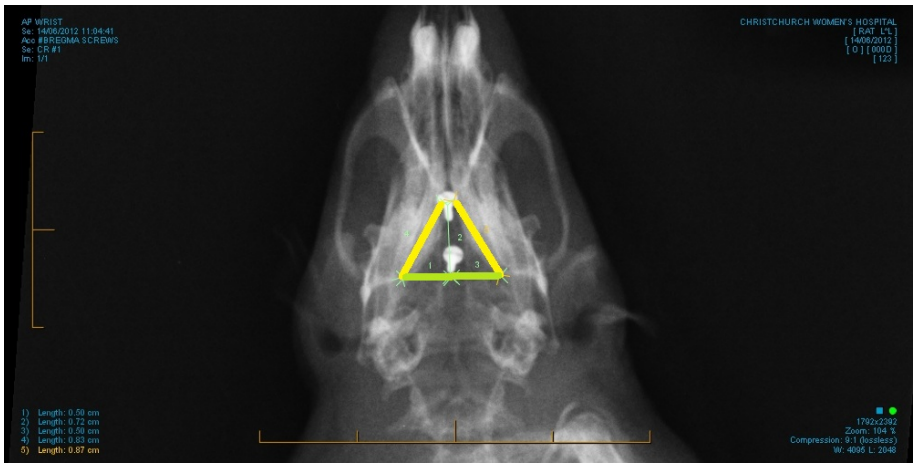

(b) Top view

Figure 5.5: *Radiographic images of euthanized rat taken at Christchurch Women's Hospital. The stainless steel pins are attached to the bregma and lambda points on the skull. The yellow lines represent the area of the hippocampus.*

5.3 MARS - CT Preview Mode

The Preview Mode is a function in the MARS CT user interface which is used to obtain an extended x-ray transmission image of the object. The function is equivalent to the pilot or scout mode scans that are performed in clinical CT scans. The pilot or scout mode scans produce radiographic images using the x-ray source on the clinical CT to locate the area of interest and verifying the pateint position before undergoing the full CT scan. This minimizes the risk of repeating the CT scan which the patient will then receive the twice the amount of

radiation dose required. The Preview Mode is accessed through the graphical user interface of the MARS CT scanner and this is shown by figure A.1 and figure A.2 in the Appendix. The length of the sample and the starting position of the scan are defined by the user prior to the Preview Mode scan. Large samples such as euthanized rats were used to test the Preview Mode scan on the MARS-CT5 and evaluate the soft tissue contrast on the Medipix 3.1 silicon quad.

The function of the Preview Mode is based on a geometric principle in projection radiography. Magnification in x-ray projection images arise due to the divergence of the x-ray beam from the focal spot to the image receptors on the detector plane. Although magnification is useful for imaging small sizes objects, it is also the source of geometric blurring as this is illustrated in figure 5.6. The focal spot of the x-ray tube is modelled as a large number of point like sources protruding through the sample and towards the detector plane (Bushberg et al., 2006). However the point sources at each ends are of subject to irregular magnication factor which can be significant enough in blurring the image. In reference to figure 5.6, the letter f represents the edge gradient blurring as a result of the x-ray beam produced at the both ends of the extended focal spot. Due to this geometrical factor, the Preview Mode only utilizes the data collected in the thin central region of the silicon quad layer, figure 5.7. The thin slices, shown by the yellow dashed lines, are progressively stitched as the horizontal translation of the sample occurs during the scan. This provides a wider x-ray transmission view of the sample.

Figure 5.9 shows the x-ray transmission image obtained from the MARS CT using the Preview Mode. The image shows a euthanized rat of the same species and weight shown in the previous set of radiographic images. In addition to the stainess steel spin attached to the bregma point, a thin aluminium plate with holes drilled in a grid pattern of 3mm $\times$ 3mm was placed around the rat‘s head. The extra attenuation of the aluminium formed bright spots in the image. The bright spots are labelled using red markers as this was done as a part of the post processing step of the image. The position of the holes were used as reference markers for scaling and locating the position of the hippocampus relative to the interaural line and bregma.

Post processing is an essential technique in improving the quality of images. Techniques

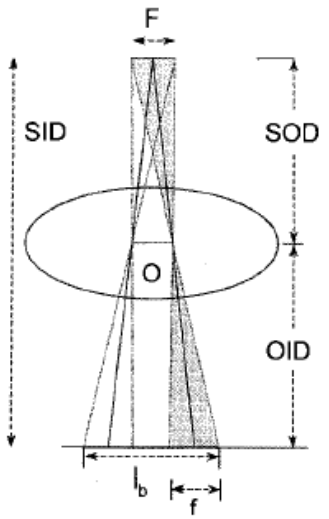

Figure 5.6: *Figure showing the geometrics of the x-ray tube. The image edges are suubject to magnifcation blurring, f, which is produced by the extended focal spot of the x-ray tube labelled as F. (Bushberg et al., 2006)*

such as flatfield correction and filtering kernels are common post processing techniques that are used in digital radiography (Davidson, 2007). The limiting factors of the Preview Mode includes malfunctioning pixels in the detector and the interchip spacing as they contribute some level of degradation in the image. The contribution of the limiting factors is shown in figure 5.8(a) where the image quality is affected by the dead pixel regions. To improve the quality and to visually differentiate between soft tissues, the smoothing filter was applied to the images obtained through the Preview Mode. Smoothing filter is a weighted mean based kernel, shown in figure 5.1, where each pixel in the image plane is replaced by the mean value of the surrounding pixels. The process is mathematically defined in equation 5.5 where the output image, $O(i, j)$, is the product between the image, I, and convolution kernel, K. The improvement as a result of the smoothing filter is shown in figure 5.8(b) where the degraded pixels within the image is averaged out and improving the soft tissue visibility of the image.

$$O(i,j) = \sum_{k=1}^{m} \sum_{l=1}^{n} I(i+k-1, j+l-1)K(k,l) \tag{5.5}$$

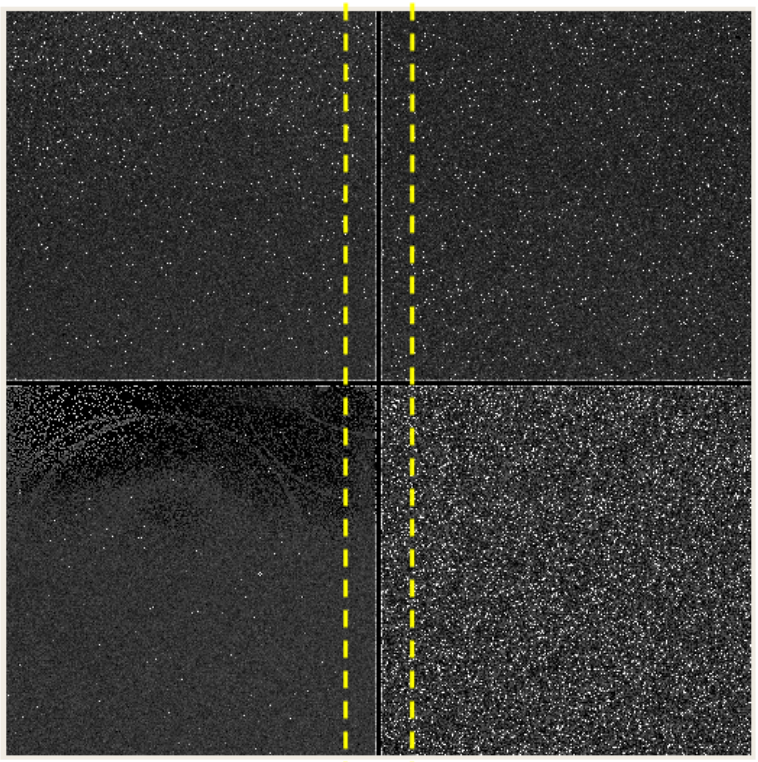

Figure 5.7: *Figure showing the Medipix 3.1 Silicon Quad detector (Q12). The yellow dotted lines represent the narrow slice region on the detector which the x-ray transmission data is used to stitch and produce an extended x-ray transmission image.*

$\frac{1}{9}$	$\frac{1}{9}$	$\frac{1}{9}$
$\frac{1}{9}$	$\frac{1}{9}$	$\frac{1}{9}$
$\frac{1}{9}$	$\frac{1}{9}$	$\frac{1}{9}$

Table 5.1: *Smoothing kernel that is convoluted with the image to produce a better quality image. This kernel is used to replace the central pixel values with the average pixel value of the surrounding pixels.*

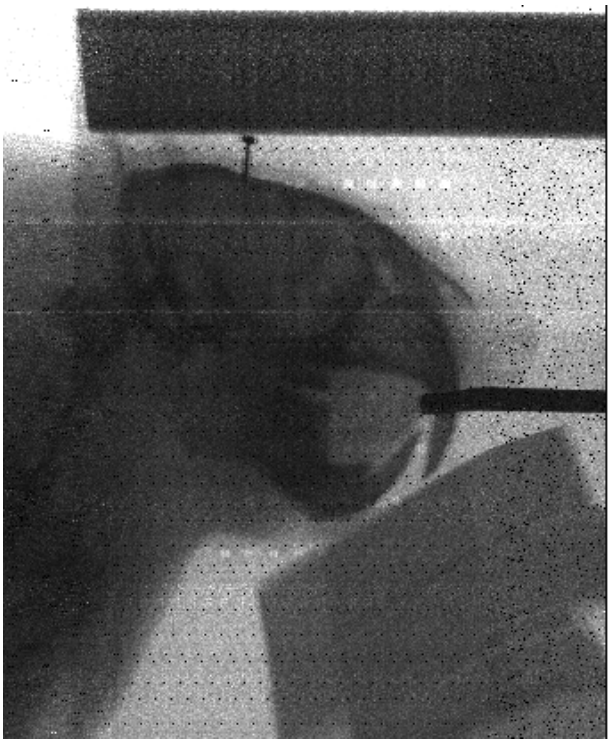

(a) Original image

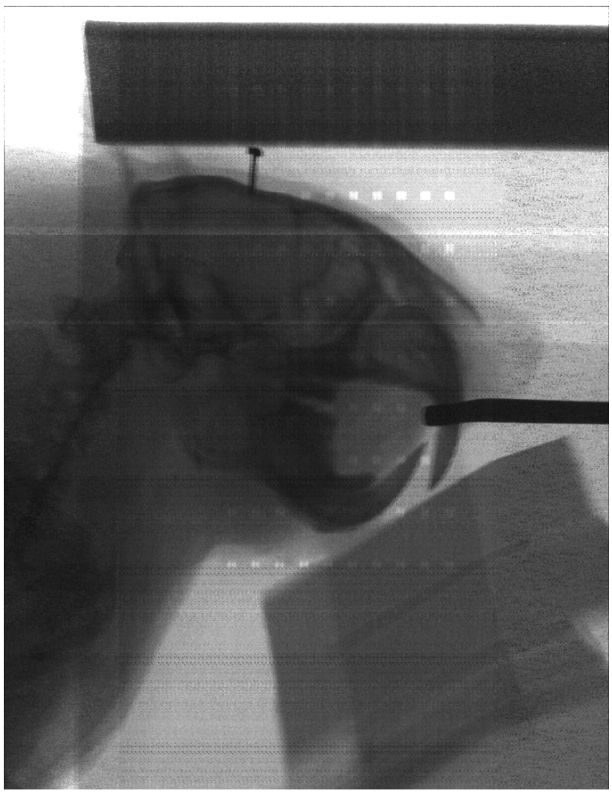

(b) Image with smooth filtering added

Figure 5.8: *Figures showing: (a) the original image produced from the MARS Preview Mode and (b) image showing the improved quality after applying the smoothing filter*

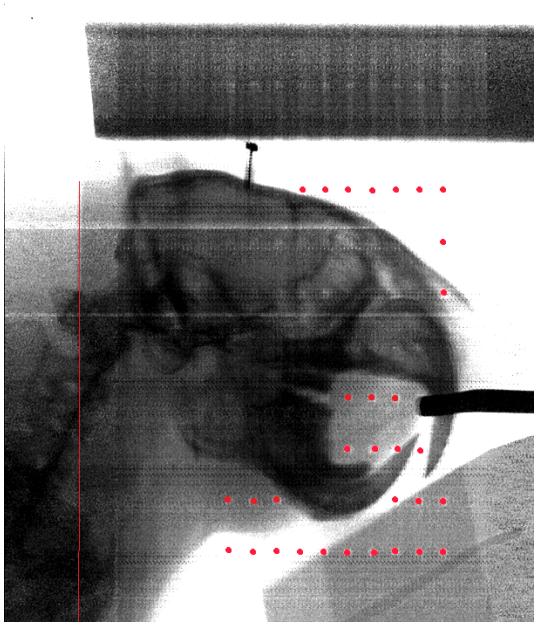

Figure 5.9: *Figure x-ray projection image taken from MARS CT-5 with the Medipix 3.1 silicon quad. The image shows an euthanized rat with steel pin attached to the bregma of the rats skull. Aluminium plate with grid pattern holes was placed around the rats head for geometric information.*

CHAPTER 6

Rat Irradiation and Histology

This chapter describes the process of the irradiation process and how the x-ray exposure to the hippocampus was measured and controlled. It also includes a section on the immunohistochemsitry process of the brain and the results obtained by viewing through a light microscope. The immunohistochemsitry was performed at the Department of Psychology, University of Canterbury.

6.1 Irradiation

A study was performed to verify the precision of the x-ray delivery through the use of the live rat holder and the lead collimators. The experimental outcome was based on whether the neurogenesis in rat brain was inhibited from the custom built setup and the ionizing radiation produced inside the MARS Spectral CT. The most important part of the experiment was fixing the rat's head onto the stereotaxic surgery bars as this required extreme precision and stability to minimize the positional variation between each rat for irradiation. The position of the ear bars and the nose bar was always kept constant. Two pairs of lead collimators were built for each dorsal and ventral hippocampuses with hand carved holes for the propagation of the x-ray. The lead collimator is shown in figure 6.1 where the hole to irradiate the hippocampus was hand carved. The position of the holes were based on the plots shown in figure 5.4, Chapter 5. The overall setup of the rat with the stereotaxic bars and colliamtors

is shown in figure 6.2.

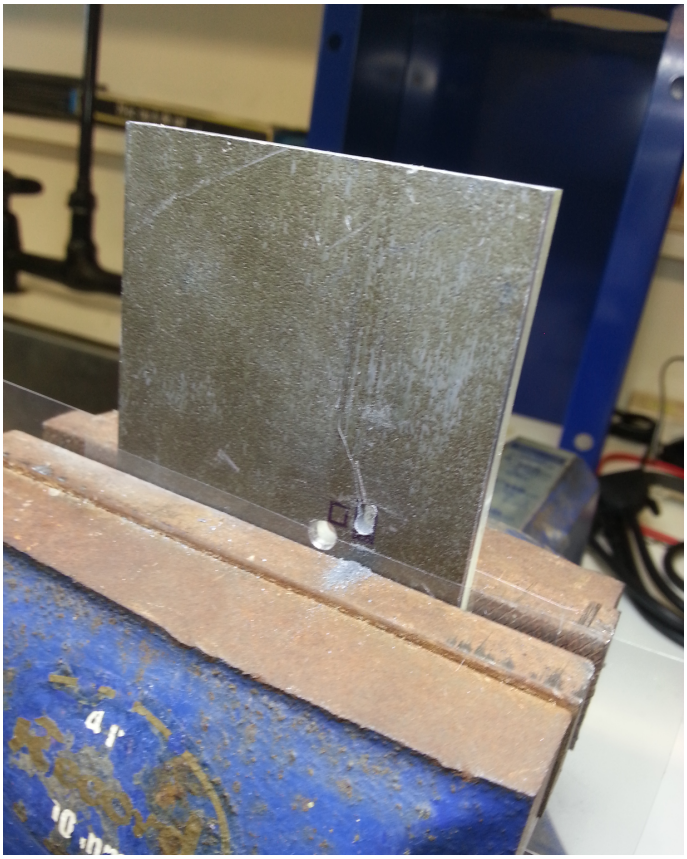

Figure 6.1: *The lead collimator used to confine the cone beam x-ray. The position of the x-ray hole was hand carved.*

Three rats were chosen for the purpose of this study and were irradiated using the MARS Spectral CT. Prior to the irradiation, the rats were prepared and injected with the BrdU as mentioned in Chapter 3. The quantity of the radiation delivered to the hippocampus was controlled using the exponential model of the depth dose curve shown in figure 4.6, Chapter 4. The depth of the hippocampus was measured using the clinical radiographs using the scale bars and the plotted area of the hippocampus. The exposure time for each lateral beam was calculated on the basis that the beam delivered the radiation to the hippocampus in both hemispheres. Figure 6.3 shows the measurements labelled the radiographic images using the scale bar at the bottom where each bar corresponds to 1cm. The depths of both hippocampus in each hemisphere were measured at 10.5mm and 15.9mm.

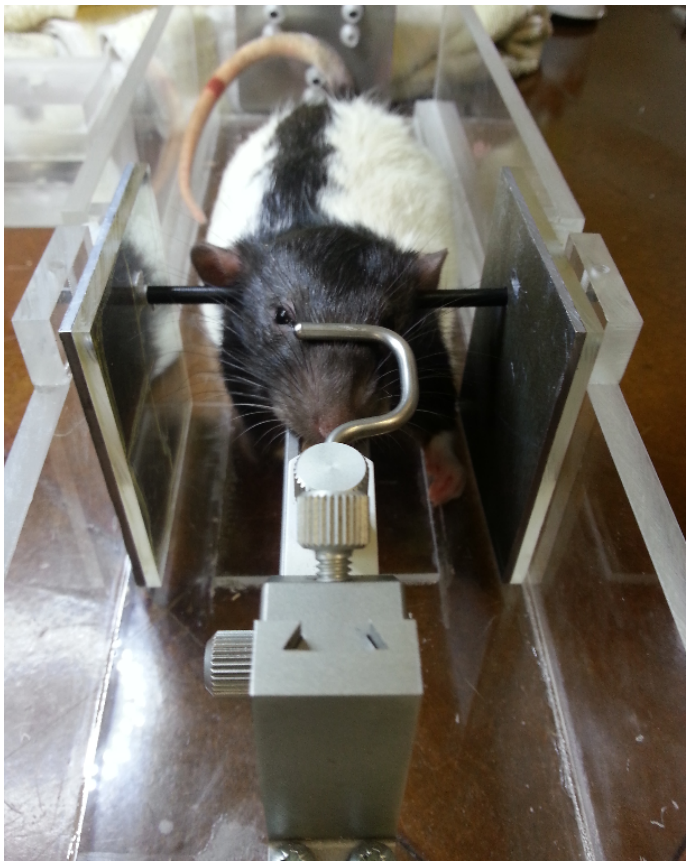

Figure 6.2: *Close up photo of the rats head fixed with the ear bars and nose bars and also the collimators which are connected with the ear bars.*

The exposure time for each lateral beam was calculated on the basis that the x-ray irradiated the hippocampus in both hemispheres. The point dose rate at each hippocampus depth was calculated using the depth dose curve and this is illustrated through figure 6.4. From the model, the point dose rate at the corresponding depths of 10.5mm and 15.9mm was calculated as 178.63mGy/min and 131.63mGy/min respectively. Assuming that the position of the rat‘s head was placed in the middle of the parallel opposing beam geometry, the point dose rate values of 178.63mGy/min and 131.63mGy/min were added together for the total point dose rate of 310mGy/min for each hippocampus. The illustration shown in figure 6.5 provides how the parallel opposing beam geometry delivers the radiation dose to both hemispheres.

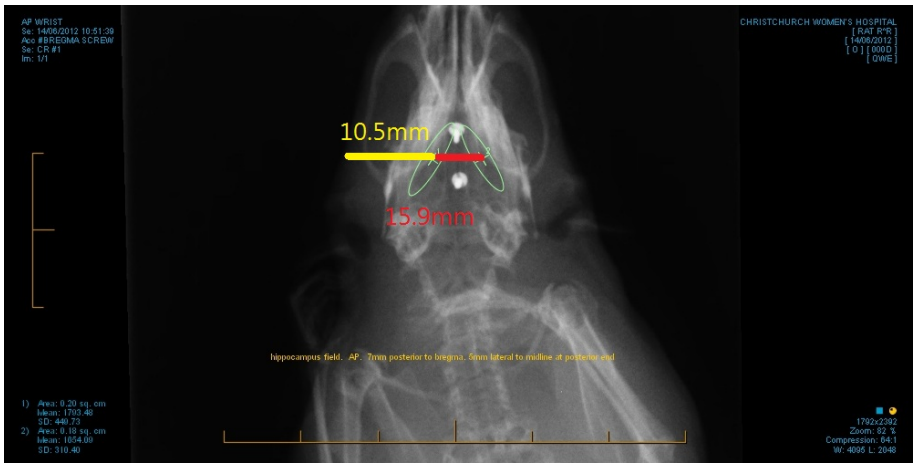

Figure 6.3: *Figure showing the measurement of the depth of the hippocampus. The depth of the hippocampus on each hemispheres was measured from the same side.*

6.2 Histology

The irradiated rats were kept alive for three weeks to see the effect of the reduced neurogenesis. In addition to the BrdU, the staining process using DCX was performed in parallel due to the numerous groups that have successfully labelled developed neurons using this specific method of staining. After three weeks, each brain was perfused and sliced into sections for immunohistochemistry and prepared on to slides to be viewed through a light microscope. However, the BrdU method of labelling the neurons did not work as it did not show any neurons within the control rat. For this study, only the brain sections stained with the DCX was analyzed.

However the microscope analysis of the prepared slides showed mixed results. One out of the three pilot rats showed sign of reduced neurogenesis in the hippocampus. The series of images shown in figure 6.7 shows the sections of the rat‘s brain with the DCX stained neurons and the developed dendrites. The density of the stained neurons and dendrites in the control rat, (a), was used to relatively compare the number of the remaining neurons in the irradiated rats. The images, (b) and (c), show the brain sections of the rat that showed positive results of reduced neurogenesis. This is seen by the reduced concentration of the neurons and the limited growth of the dendrites compared to the control rat.

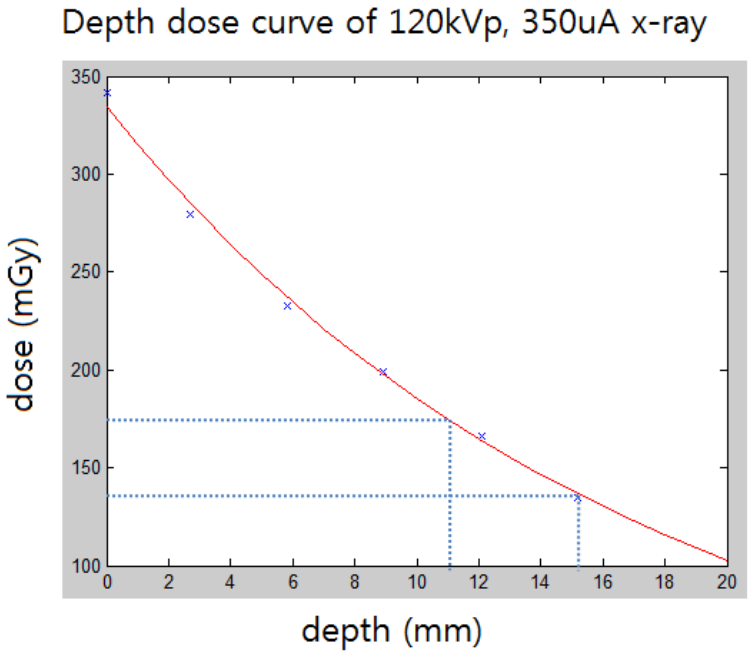

Figure 6.4: *Graph showing the depth dose curve with the labeled depths of the hippocampus at both hemispheres*

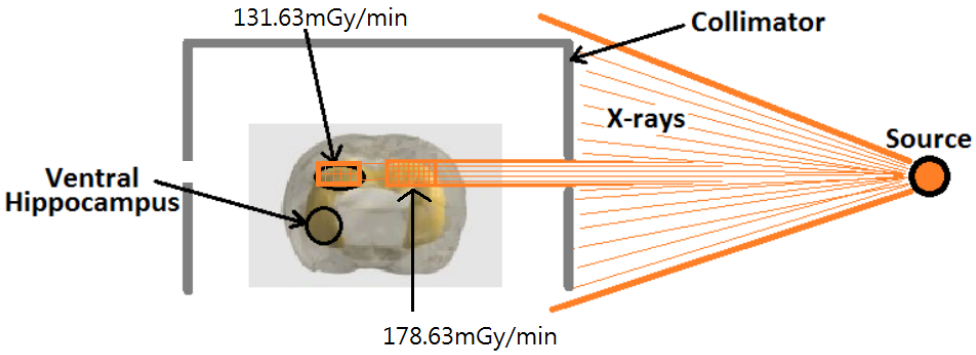

Figure 6.5: *Diagram illustrating the point dose rate from a single lateral beam in both hemispheres. The values will be flipped around with the x-ray source on the opposite side.*

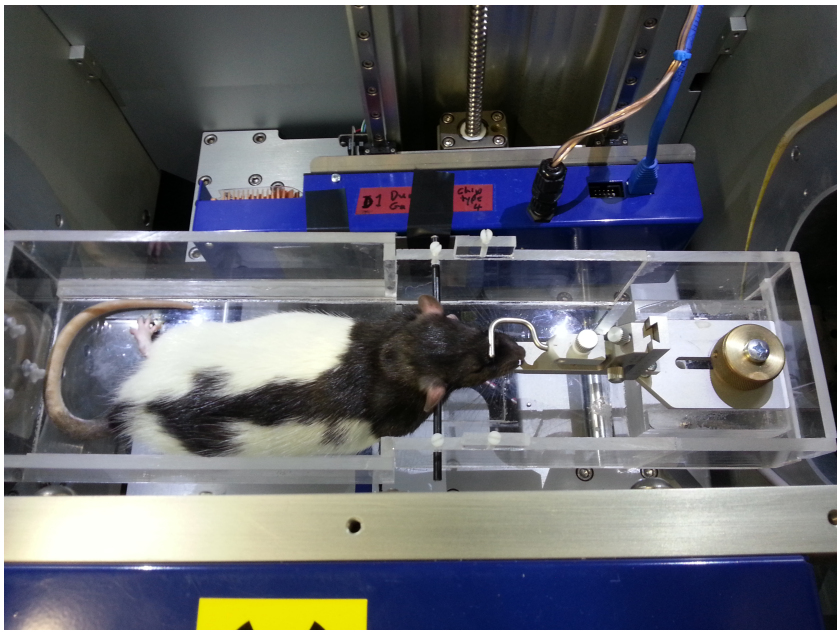

Figure 6.6: *Showing the rat positioned inside the scanner fixed in place on the live animal holder. It is assumed that the position of the head held by the stereotaxic bars is in the centre of the opposing parallel beam geometry.*

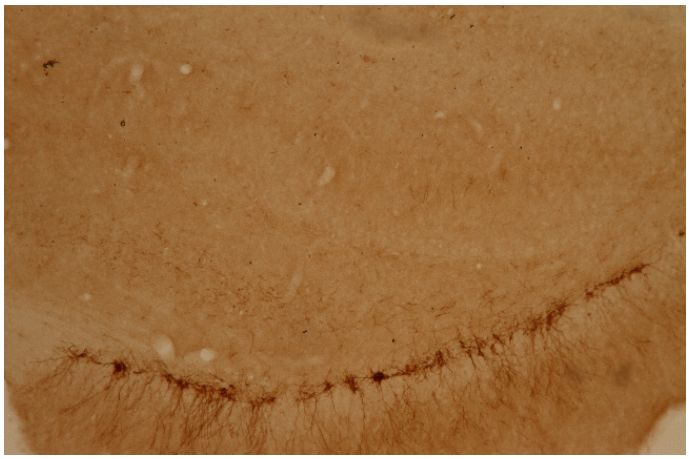

(a) control

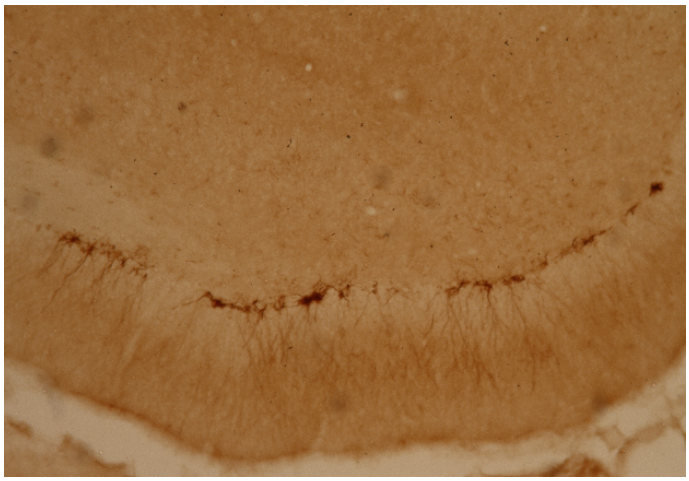

(b) (irradiated)

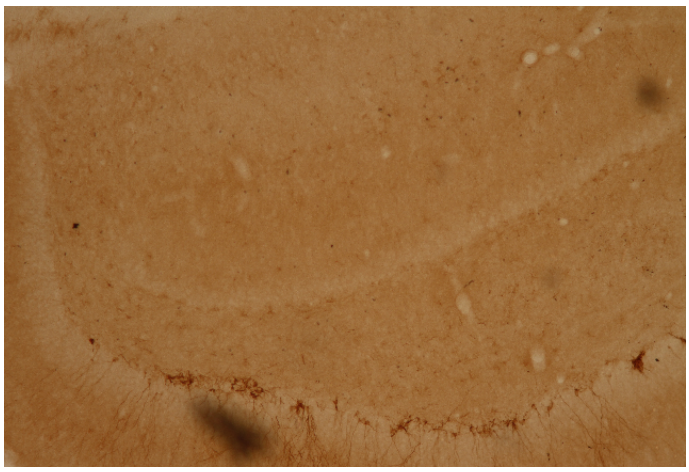

(c) (irradiated)

Figure 6.7: *Light microscopy image of the brain section of the brain stained with DoublecortinX. (a) unirradiated control rat (b) irradiated rat showing small reduction in the number of neurons (c) a section in the irradiated rat brain which showed very low number of neurons showing signs of reduced neurogenesis.*

CHAPTER 7

Conclusion

This chapter concludes the thesis by summarizing the main objectives and the results that were obtained through the work. In addition, some relevant future outlook of the MARS Spectral CT and its applications with small animal radiotherapy is discussed.

7.1 Summary

This thesis was based on the work of analyzing the potential of the MARS Spectral CT to be used for irradiating small animals. The current active versions of the scanner have not been designed for the purpose of small animal irradiation. Series of developmental procedures were taken to equip the scanner with the necessary tools required for the irradiation process. Tools such as live rat holder and the lead collimators was important to accurately deliver the radiation dose to the hippocampus. The accuracy of the beam delivery was achieved through the positioning of the rat‘s head onto the live animal holder and also through the design of the collimators where the exact position of the hippocampus was carved out ont he lead collimator for the x-ray to go through. The localization of the hippocampus was based on the anatomical landmarks; bregma, lambda and the interaural line which was used to design the collimators for each dorsal and ventral hippocampus.

7.2 Discussion

The Medipix 3.1 has been the subject of recent accomplishments within the MARS group. In particular, the Preview Mode has benefited from the Medipix 3.1 such as the scanning time and contrast to noise ratio. Previously when using the Medipix 3.0 detector, the Preview Mode scan of the rat's head with a length of 60mm and height of 60mm took an average time of 18 to 20 minutes. The efficiency of the Preview mode, when converted to the Medipix 3.1, vastly improved as it showed a near three fold improvement of 7 to 8 minute scanning time. The limitation of using the silicon quad detector, shown in figure 5.7, Chapter 5, is the inter-chip spacing. Due to the Preview Mode utilizing a narrow slice in the central region of the detector, small areas from all four chips were part of the narrow slice which contributes to the image degradation. However, the scanning time of the Preview Mode scan can be improved further by improving the detector processing time. The fact that the Preview Mode scan only utilizes a narrow slice, the unused areas on the silicon quad chips still contributes to the processing time during the readout process. By actively turning off the unused areas on the silicon chips, the detector processing time will be improved resulting in reduced scanning time.

The limitation that was experienced during this study was the physical setup of the live rat onto the line animal holder and the accuracy of the designed collimators for targeting the hippocampus. Because of the novelty of this experiment within the group, the current active versions of the MARS CT scanners are not designed for the purpose of small animal irradiation. Although the live animal holder is specifically designed to hold the rats in constant positions inside the MARS scanner, there are uncertainties in the stability of the system due to minute design and construction errors. The fact that the hippocampus lies only several millimetres away from the interaural line, marginal errors in the alignment of the collimators in respective to the position of the position of the rat's head can be a significant factor of irradiating a non-target region within the brain. The total uncertainty in the dose values measured using the Gafchromic system consists of several factors such as: reference dosimetery system calibration, dosimeter temperature and calibration curve (Mehta & Parker, 2011).

There have been reported documents covering the difficulties involving the BrdU method of labelling neurons within the hippocampus. There have been suggestions that the thymidine component of the BrdU get into the brain less efficiently in adult animals than in foetuses because of the difference in blood flow metabolism and development of blood brain barrier

(Gould & Gross, 2002). Also recent studies have shown that standard laboratory conditions might be a limiting factor as the number of BrdU labelled cells is lost between 1 and 3 weeks after BrdU labelling (Tanapat et al., 1998).

7.3 Future Outlook

With the MARS Version 5 nearly in its final stages of development, the limitations of positioning the rat's head and the collimators will be much improved. Some of the developmental work of the new version is shown in figure 7.1. With the added features in the scanner; such as the x-y translational stage and automated shutters, it removes the necessity of an additional collimator to confine the size of the x-ray beam. Combined with the x-ray transmission images taken from the Preview Mode, the MARS Version 5 scanner can expand towards the field of image guided irradiation applications where the subvolume within small animals can selectively targeted using the x-ray transmission image and controlling the position of the x-ray shutter openings.

7.4 Conclusion

The platform of small animal irradiation is a challenging field. The accuracy and precision of the x-ray beam delivery relies heavily on the physical setup of the animal and also the technical specifications of the platform used for irradiation. Variables such as small field sizes and kilovoltage beam dosimetry are complex parameters that need to be verified by further experiments. The sign of reduced neurogenesis has been seen in one rat which proves that the MARS CT scanner is a suitable platform for this specific application. With the improved setup provided from the upcoming MARS V5 scanners, a more accurate method of delivering the radiation will be planned and initiated. In addition, this will open novel applications of radiobiological research and other small animal irradiation experiments resulting in more collaborative projects performed within the MARS group.

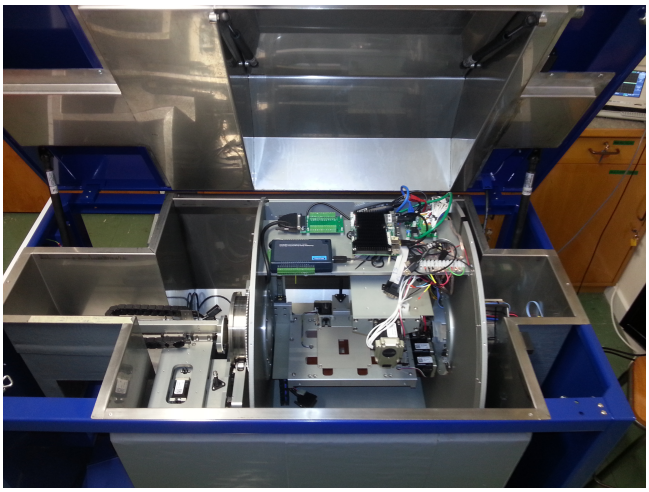

(a) CR-10 in its development stage

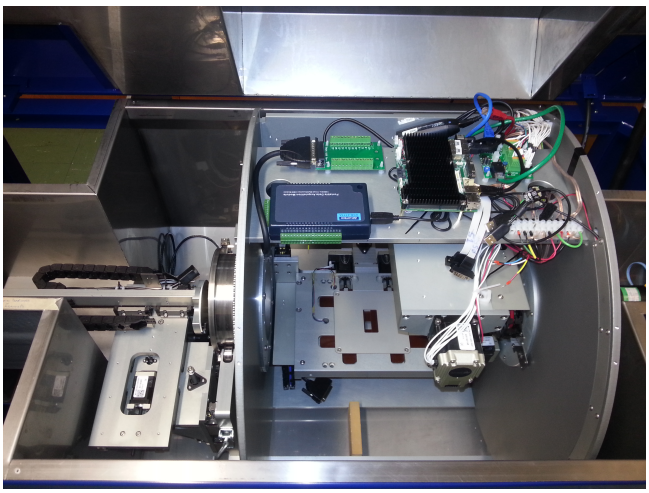

(b) CR-10 in its development stage

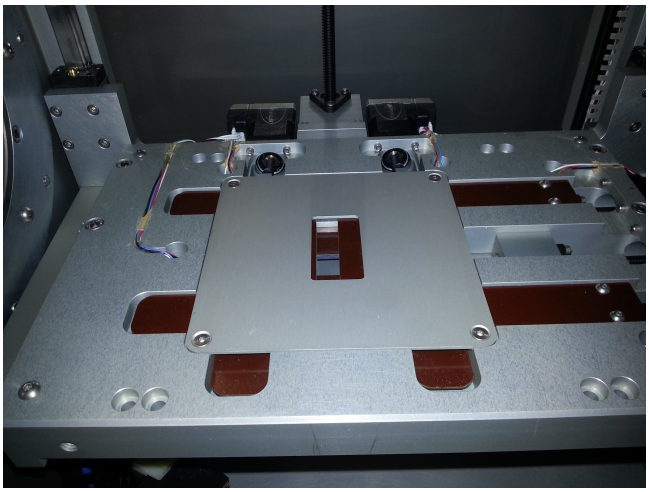

(c) Automated shutters

Figure 7.1: *The MARS-CR10 currently in its final stages of development. The gantry, (a) and (b), and the motorized shutters, (c), are shown.*

References

Altman, J., & Das, G. D. (1965). Autoradiographic and histological evidence of postnatal hippocampal neurogenesis in rats. *J. Comp. Neur*, *124*, 319–336.

Bolus, N. E. (2001). Basic review of radiation biology and terminology. *Journal of Nuclear Medicine Technology*, *29*, 67–73.

Bushberg, J. T., Seibert, J. A., Leidholdt, E. M., & Boone, J. M. (2006). *The essential physics of medical imaging.* Lippincott Williams and Wilkins.

Butler, P., & Butler, A. (2013). *Mars bioimaging.* Retrieved from `http://www.marsbioimaging.com/mars/`

Davidson, R. (2007). *Radiographic contrast-enhancement masks in digital radiography.* Unpublished doctoral dissertation, University of Sydney.

Davisson, C. (1965). Interaction of gamma radiation with matter. *Alphta Beta and Gamma ray Spectroscopy*, *1*, 37.

Deng, W., Amione, J., & gage, F. (2010). New neurons and new memories: how does adult hippocampal neurogenesis affect learning and memory. *Nature Reviews Neuroscience*, *11*, 339–350.

Gafchromic xr-qa dosimetry film product brief [Computer software manual]. (n.d.).

Gage, F., Kempermann, G., & Song, H. (2008). *Adult neurogenesis.* CSHL Press 2008.

Gould, E., & Gross, C. (2002). Neurogenesis in adult mammals: some progress and problems. *The Journal of Neuroscience*, *22*, 619–623.

Hounsfield, G. N. (1973). Computerized transverse axial scanning (tomography): Part 1. description of system. *British Journal of Radiology*, *46*, 1016–1022.

il Ming, G., & Song, H. (2011). Adult neurogenesis in the mammalian brain: Significant answers and significant questions. *Neuron*.

Jevremovic, T. (2009). *Nuclear principles in engineering, second editiom.* Springer Science.

Joiner, M., & van der Kogel, A. (2009). *Basic clinical radiobiology.* Edward Arnold.

Khan, F. (2003). *The physics of radiation therapy.* Williams & Wilkins.

Khoshnazar, K., M, J., & S, A. N. (2012). Gamma radiation-induced impairment of hippocampal neurogenesis, comparison of single and fractionated dose. *International Journal of Morphology*, *30*, 145–149.

Leuner, B., Gould, E., & Shors, T. J. (2006). Is there a link between adult neurogenesis and learning? *Hippocampus*, *16*, 216–224.

Ma, C. M., Coffey, C. W., DeWard, L. A., Liu, C., Nath, R., Seltzer, S. M., & Seuntjens,

J. P. (2001). Aapm protocol for 40–300 kv x-ray beam dosimetry in radiotherapy and radiobiology. *American Association of Physicists in Medicine*, *28*, 868–893.

Matinfar, M., Ford, E., Iordachita, I., Wong, J., & Kazanzides, P. (2009). Image guided small animal radiation research platform: calibration of treatment beal alignment. *Physics in Medicine and Biology*, *54*, 891–905.

McEwan, A. (2004). *Nuclear new zealand.* Hazard Press Limited.

Mehta, K., & Parker, A. (2011). Characterization and dosimetry of a practical x-ray alternative to self shielded gamma irradiators. *Radiation Physics and Chemistry*, *80*, 107–113.

Motomura, A., Bazalova, M., Zhou, H., & Graves, E. (2009). Investigation of the effects of treatment planning variables in small animal radiotherapy dose distributions. *Medical Physics*, *37*, 590–599.

Park, M.-K., Kim, S., jung, U., Kim, I., Kim, J.-K., & Roh, C. (2012). Effect of acute and fractionated irradiation on hippocampus neurogenesis. *Molecules*, *17*, 9462–9468.

Paxinos, G., & Watson, C. (1997). *The rat brain in stereotaxic coordinates.* Academic Press Limited.

Paxinos, G., Watson, C., Pennisi, M., & Topple, A. (1985). Bregma, lambda and the interaural midpoint in stereotaxic surgery with rats of different sex, strain and weght. *Journal fo Neuroscience Methods*, *13*, 139–143.

Pordgorsak, E. (2005). *Radiation oncology physics: A handbook for teachers and students.* Vienna, Austria: IAEA.

Rodriguez, M., Zhou, H., Keall, P., & Graves, E. (2009). Commissioning of a novel microct/rt system for small animal conformal radiotherapy. *Physics in Medicine and Biology*, *54*, 3727–3740.

Rola, R., Raber, J., Rizk, A., Otsuka, S., VandenBerg, S. R., Morhardt, D. R., & Fike, J. R. (2004). Radiation-induced impairment of hippocampal neurogenesis is associated with cognitive deficits in young mice. *Experimental Neurology*, *188*, 316–330.

Schindler, M. K., Bourland, J. D., Forbes, M. E., Hua, K., & Riddle, D. R. (2011). Neurobiological responses to stereotacticc focal irradiation of the adult rodent hippocampus. *Journal Neurobiological Sciences*, *306*, 129–137.

Sharma, A. (2007). *Temporal profile of pathological changes and gene regulation in a kainic acid induced fischer 344 rat model of mesial temporal lobe epilepsy.* Unpublished doctoral dissertation, Purdue University.

Snyder, J. S., Hong, N. S., Mcdonald, R. J., & Wojtowicz, J. M. (2005). A role for adult neurogenesis in spatial long-term memory. *Neuroscience*, *130*, 843–852.

Tan, Y. F., Rosenzweig, S., Jaffray, D., & Wojtowicz, J. M. (2011). Depletion of new neurons by image guided irradiation. *Frontiers in Neuroscience*, *5*, Article 59.

Tanapat, P., Galea, L., & Gould, E. (1998). Stress inhibits the proliferation of granule cell precurosrs int he developing dentate gyrus. *International Journal of Developmental Neuroscience*, *16*, 235–239.

Verhaegen, F., Granton, P., & Tryggestad, E. (2011). Small animal radiotherapy research platforms. *Physics in Medicine and Biology*, *56*, 55–83.

Winocur, G., Wojtowicz, J. M., Sekeres, M., Snyder, J. S., & Wang, S. (2006). Inhibition of neurogenesis intereferes with hippocampus-dependent memory function. *Hippocampus*, *16*, 296–304.

Wong, J., Armour, E., Kazanzides, P., Iordachita, I., Tryggestad, E., Deng, H., ... DeWeese, T. L. (2008). A high resolution small animal radiation research platform (sarrp) with x-ray tomographic gudiance capabilities. *International Journal of Radiation Oncology and Biology and Physics*, *71*, 1591–1599.

Woo, M., & Nordal, R. (2006). Commissioning and evaluation of a new commercial small rodent x-ray irradiator. *Biomedical imaging and intervention journal*, *2*, 1–5.

Zainon, R., Butler, A., Cook, N., Butzer, J., Scleich, N., de Ruiter, N., ... Butler, P. (2010). Construction and operation of the mars-ct scanner. *Inernetworking Inodneisa Journal*, *2*, 3–10.

Zhou, H., Rodriguez, M., van den Haak, F., Nelson, G., Jogani, R., Xu, J., ... Graves, E. E. (2010). Development of microct-based image-guided conformal radiotherapy system for small animals. *International Journal of Radiation Oncology and Biology and Physics*, *78*, 297–305.

APPENDIX A

User Interfaces

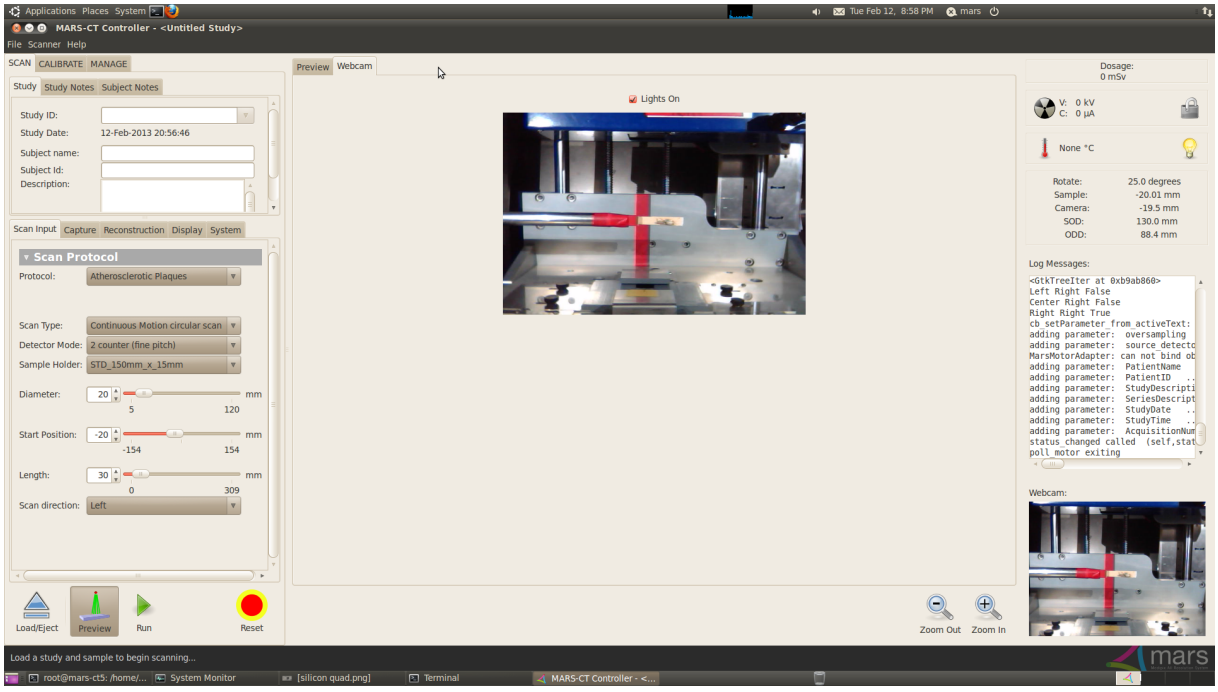

Figure A.1: *Figure showing the graphical user interface used in the MARS Spectral CT. The current system has two scan modes; Preview Mode and Scan Mode.*

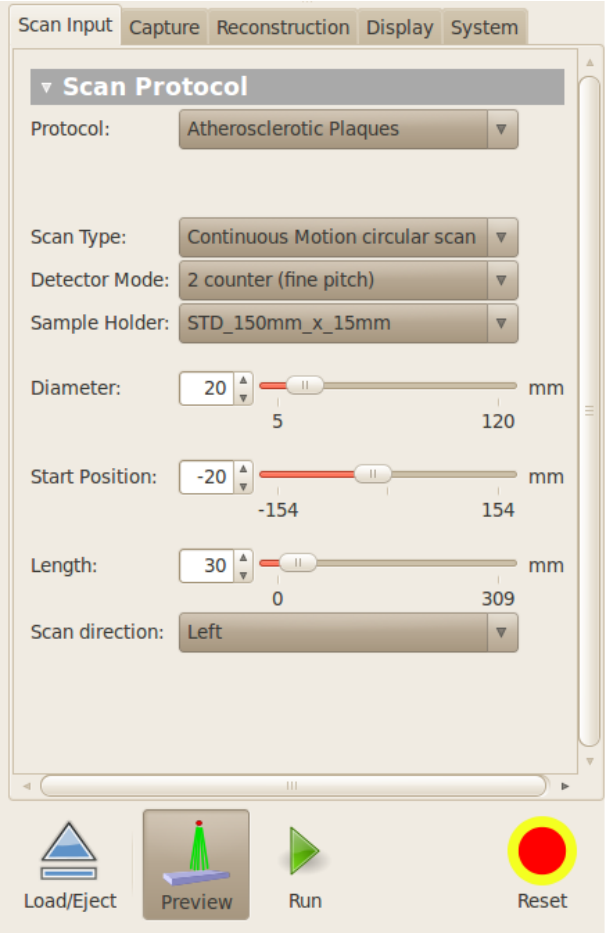

Figure A.2: *The main control panel used for setting up scans in the MARS Spectral CT. The Preview Mode requires the user to define the diameter, start position and length of the sample. The Run button is clicked to initate the scan.*